GERMAN - MONGOLIAN INSTITUTE FOR RESOURCES AND TECHNOLOGY

The present work was submitted to the Faculty of Engineering

INNOVATIVE TECHNOLOGIES FOR PRODUCING COPPER CATHODES FROM COPPER CONCENTRATES

Master Thesis

by

Munkhtuya Ganbat

Master of Science in Resource and Technology

Supervisor 1 / Examiner 1 **Prof. Dr. Battsengel Baatar**

Supervisor 2 / Examiner 2 **Dr. Purev-Ochir Togtokhbaatar**

Ulaanbaatar/Mongolia, 2025.12.19

Statutory Declaration

Ganbat, Munkhtuya	M2420004
Last Name, First Name	Student ID Number

I hereby affirm instead of an oath that I provided the submitted master thesis,

INNOVATIVE TECHNOLOGIES FOR PRODUCING COPPER CATHODES
FROM COPPER CONCENTRATES

I did not use any sources other than those stated. In case the work is additionally submitted on a data medium, I declare that the written and the electronic form are completely identical. The work was not submitted in the same or similar form to any examination authority.

Ulaanbaatar, Mongolia, 2025.12.19

Place, Date

Signature

Contents

Statutory Declaration 2
ACKNOWLEDGEMENT 6
ABSTRACT 7
CHAPTER 1. INTRODUCTION 8
1.1 Global copper industry overview 10
1.2 Copper concentrate sources and mineralogy 16
1.3 Objective of the thesis 19
1.4 Structure of the Thesis 28
CHAPTER 2. LITERATURE REVIEW 29
2.1 Introduction 29
2.2. Surface passivation mechanisms in chalcopyrite leaching 30
2.3. Advanced oxidative leaching strategies to overcome kinetic limitations 35
CHAPTER 3: METHODOLOGY 37
3.1 Introduction 37
3.2 Experimental Setup and Conditions 38
3.3 Analytical Techniques and Data Collection 60
3.4 Data Analysis and Calculations 60
CHAPTER 4: RESULTS AND DISCUSSION 64
CONCLUSIONS 75
CHAPTER 5: ECONOMIC EVALUATION 75
5.1 Scoping study for a copper hydrometallurgical plant 75
5.2. Annual Net Profit Summary 79
5.3 Environmental Significance (ESG) 79
SUMMARY 81
REFERENCES 85

LIST OF FIGURES

FIGURE 1. CIRCULAR ECONOMY CONCEPT (HTTPS://WWW.ERA-MIN.EU/) 13
FIGURE 2. GLOBAL COPPER DEMAND INTENSITY 14
FIGURE 3. FORECAST OF REFINED METAL DEMAND, COPPER METAL CONTENT (HATCH) 15
FIGURE 4. ERDENETIIN OVOO DEPOSIT ORE BODY 21
FIGURE 5. SUPERGENE ENRICHMENT (LEVINSON,1980) 25
FIGURE 6. EMC GENERAL TECHNOLOGY SCHEMA 26
FIGURE 7. EMC ORE THROUGHPUT AND PRIMARY COPPER GRADEER CONTENT 27
FIGURE 8. MASS OF COPPER CONCENTRATE AND MOLYBDENUM CONCENTRATE 28
FIGURE 9. THE PROPOSED DISSOLUTION AND PASSIVATION MECHANISMS OF THE CHALCOPYRITE LEACHING SYSTEM (JIANG, L., LENG, H., & HAN, B., 2023) 31
FIGURE 10. CATEGORY OF FRACTION CONCENTRATE 45
FIGURE 11. PANORAMIC RESULT OF THE SAMPLE 46
FIGURE 12.COPPER ELEMENTAL DEPORTMENT BY MINERAL PHASE 47
FIGURE 13. SAMPLE AND LEACH SOLUTION PREPARATION 57
FIGURE 14. ARRHENIUS PLOT 62
FIGURE 15. EFFECT OF TEMPERATURE ON CHALCOPYRITE LEACHING RECOVERY 63
FIGURE 16. MASS OF COPPER IN PSL, MG 65
FIGURE 17. EXPERIMENT WITH AMMONIUM PERSULFATE 68
FIGURE 18. SAMPLE OF AMMONIUM PERSULFATE EXPERIMENT 69
FIGURE 19.EXPERIMENT PROCESS OF WITH IODINE 71
FIGURE 20. EFFECT OF TEMPERATURE AND OXIDIZER ON COPPER EXTRACTION LEACHING SYSTEM 72
FIGURE 21. THE EXPERIMENT TEMPERATURE IS GETTING UP 73
*FIGURE 22. LABORATORY EXPERIMENTAL RESULTS ..... **ERROR! BOOKMARK NOT DEFINED.***

LIST OF TABLES

TABLE 1. COPPER DEPOSIT TYPES (CROWSON, 2012) 17
TABLE 2.MINERAL COMPOSITION BY ENRICHMENT ZONES 23
TABLE 3. MINERALOGICAL INTERACTIONS 33
TABLE 4. IMPACT OF CO-EXISTING SULFIDE MINERALS ON FLOTATION PERFORMANCE 34
TABLE 5.OXIDATIVE LEACHING STRATEGIES 35
TABLE 6 . COPPER CONCENTRATES MINERAL XRD REPORT 41
TABLE 7. SIZE FRACTIONATED ELEMENTAL ANALYSIS 43
TABLE 8. ELEMENTAL MASS OF THE SAMPLE 44
TABLE 9. COMPARATIVE MINERALOGICAL COMPOSITION BY SIZE FRACTION 46
TABLE 10. ELEMENTAL MASS OF COPPER CONCENTRATE 67
TABLE 11. TOTAL CAPITAL OPERATING EXPENDITURE (CAPEX/OPEX) 76
TABLE 12. THERMAL ENERGY DEMAND 78
TABLE 13.STAFFING STRUCTURE 78
TABLE 14. CONSOLIDATED ANNUAL NET PROFIT SUMMARY 79

Terminology

AAS	Atomic Absorption Spectroscopy
XRD	X-ray powder diffractometer
PLS	Pregnant Leach solution

ACKNOWLEDGEMENT

First and foremost, I extend my sincere thanks to Prof. Dr. Battsengel Baatar and Dr. Purev-Ochir Togtokhbaatar for generously sharing their expertise and experience during this research.

I am profoundly grateful to Erdenet Mining Corporation and GMIT for providing the opportunity to study the technology for leaching chalcopyrite-dominant copper concentrate and for offering the specific research topic. Their support laid the foundation for this work.

A special expression of gratitude goes to Dr. Purev-Ochir Togtokhbaatar for his support, guidance, and organization in carrying out the experimental work at the GMIT Chemistry Laboratory. His technical expertise and support were crucial in generating the experimental data and understanding the technological process that forms the core of this thesis.

Finally, I express my deep appreciation to my family for their unwavering support, patience, and encouragement throughout my academic journey.

ABSTRACT

The leaching process of chalcopyrite-dominated copper ore exhibits slow electron-transfer kinetics. The leaching of copper concentrates rich in chalcopyrite remains one of the main limitations of modern hydrometallurgy, due to slow electron-transfer kinetics, surface passivation from elemental sulfur or jarosite type precipitates, and the high acid consumption typically required to maintain a stable leaching process. In line with the global sustainability agenda's top priorities, developing environmentally friendly, low sulfuric acid consumption, high efficiency leaching systems has become increasingly important. In recent years, international studies have identified iodine-based oxidizing environments as a reliable alternative. This is because iodine (I^-/I_2) participates in a reversible oxidation–reduction cycle, does not release toxic gases, and does not accumulate in the environment, making it regarded as an environmentally friendly oxidant in modern green hydrometallurgical technology. In this study, sulfuric acid (H_2SO_4), hydrochloric acid (HCl), and nitric acid (HNO_3) are the three main acidic media, chloride complex formation, and strong oxidation degradation pathways, respectively. To enhance oxidation, ammonium persulfate $(NH_4)_2S_2O_8$), iodine (I_2) was added to each system at the same concentration, creating a mixed acid–oxidant leaching environment. In the next experimental stage, iodine was added to evaluate the synergistic effect via the $I_2/I^-/Fe^{3+}$ redox cycle. (I_2/I^-) was added and found to accelerate chalcopyrite oxidation, break down the passivation layer, and significantly reduce acid consumption. International studies show that iodide-assisted systems reduce acid and oxidant consumption by 20–40% and improve copper leachability from ore minerals, as evidenced by experimental and research results. Chemical leaching experiments were conducted at controlled temperatures of 20 °C, 50 °C, and 70 °C, and the kinetic characteristics, accelerated by the activation energy and temperature effects, were determined for each acid–oxidant combination. By integrating mineralogical observations, kinetic analyses, and thermodynamic conclusions, the mechanism by which mixed acid–oxidant–iodine systems enhance copper dissolution in the environment without causing harm was elucidated. These experimental results provide theoretical and practical insights for developing new generation hydrometallurgical processes that deliver improve copper recovery with low reagent consumption and

reduced environmental impact, and offer a scientifically based alternative for dissolving copper concentrate.

CHAPTER 1. INTRODUCTION

Sustainable and optimal mining production requires implementing production planning, technological processes, and final product processing technologies that account for the characteristics of mineral raw materials, market demand for products, and economic factors.

Based on technological research on deposits, developing a production plan to produce copper concentrate and sell non-metallic copper in the market has significant financial and other benefits. Mineral resources are depleting reserves. Therefore, there is a continuous need to explore and implement potential technological solutions during the extraction process.

Copper extraction and processing utilize a diverse range of beneficiation and refining methodologies, contingent on the ore's geotechnical characteristics and technological feasibility. Investigating traditional pyrometallurgical and hydrometallurgical processes, evaluating the application and compatibility of novel solvents (lixiviants), and implementing innovations such as advanced SX-EW technologies have become imperative research directions in the current landscape.

Chalcopyrite ($CuFeS_2$) is the most abundant and widely distributed copper bearing mineral. After chalcopyrite and its associated minerals are upgraded by froth flotation, the resulting concentrate is typically subjected to hydrometallurgical processing. When chalcopyrite dominant concentrates are processed using hydrometallurgical technologies, their behavior is strongly governed by the surface chemical states, crystallographic orientation, and redox induced transformations that develop during grinding, flotation, and subsequent processing stages; these factors directly influence copper dissolution kinetics and passivation phenomena. These surface and redox characteristics are intrinsically linked to the crystal structure of chalcopyrite, particularly the atomic arrangement within the unit cell and the generation of broken bonds and coordination changes on specific crystallographic planes, which govern surface reactivity and passivation mechanisms. Figure 1 shows the crystal structure

of chalcopyrite, showing the arrangement of Cu–Fe–S atoms within the unit cell. (Tao & Dongwei, 2014)

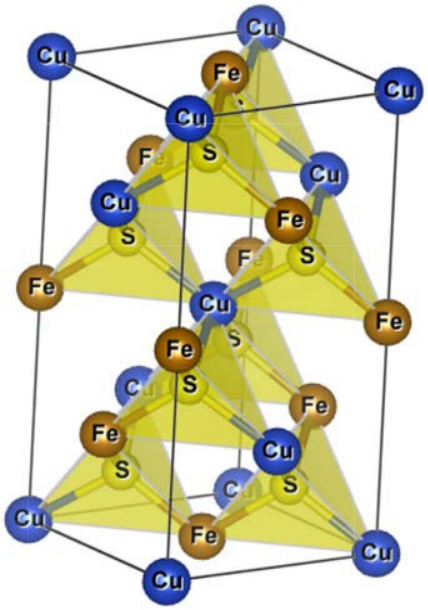


Figure 1. Crystal structure of chalcopyrite

The determination of oxidation states in metal sulfides is not merely a theoretical exercise; it is fundamental to understanding the crystal-chemical properties that dictate mineral formation, breakdown mechanisms, and behavior during industrial processing. Within the Cu–Fe–S system, chalcopyrite ($CuFeS_2$) stands as the most significant phase due to its status as the world's primary copper source.[3] However, despite its industrial importance, the precise electronic configuration of its constituent ions has remained a subject of intense scientific scrutiny. Structurally, chalcopyrite crystallizes in the tetragonal space group. It adopts a derivative of the zincblende structure, where the cations (Cu and Fe) and anions (^{8}S) are four-coordinate, forming a network of corner-sharing tetrahedra. In this lattice, the copper and iron ions are systematically ordered into alternate cation sites, which underpins the mineral's semiconducting properties. (Pearce et al., 2006)

The crystal structure of chalcopyrite is tetragonal, in which each sulfur ion is coordinated by four iron or copper ions. In natural systems, the oxidation states of the metal ions tend to form more complex, alloy-like electronic configurations rather than simple ionic states, and their actual valences often deviate from conventional

expectations. Within copper sulfides, part of the sulfur may be present as S_2^{2-} species, contributing to structural stability and enabling the solid to behave as a metallic conductor under certain conditions. (Lundström, n.d.)

The objective of this study is to characterise the refining of copper concentrates, waste management control, and post-process purification, and to define strategies to mitigate environmental hazards and assess regulatory impacts. Furthermore, this research contributes to process intensification by investigating electrode material types, quality, and advanced electrochemical solutions in metallurgical production, with a specific focus on enhancing cathode substrate durability, deposit quality, and energy efficiency.

From an economic perspective, the role of copper recycling was examined through innovations in scrap classification, alloy separation, and valuation methodologies. In the modern technological era, emerging trends facilitate improvements in reaction kinetics, selective separation, and smart manufacturing, fostering adaptive conditions across all stages of production. These advancements are strategically oriented towards addressing current industry challenges.

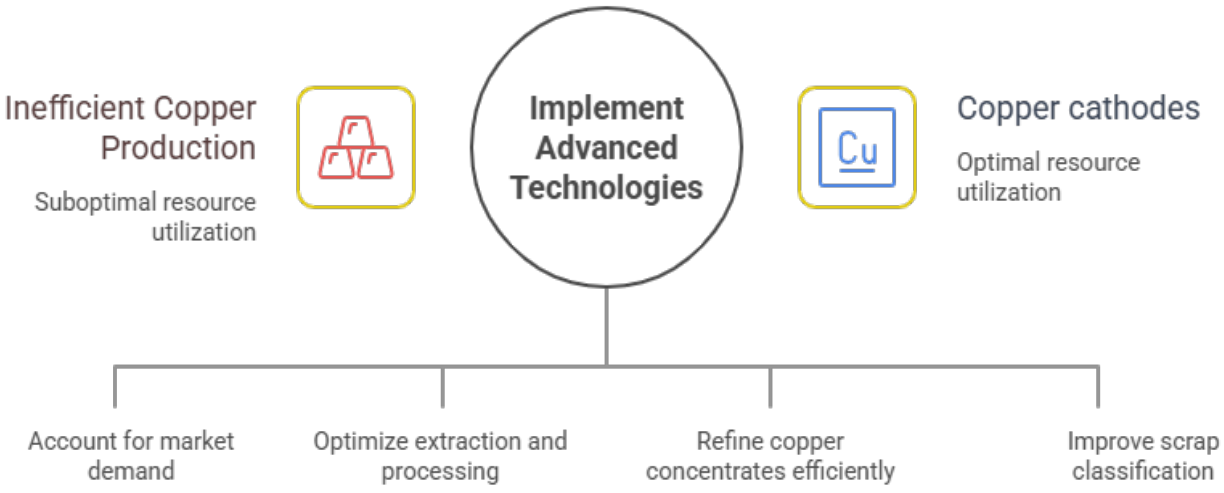


Figure 2.Optimization of copper production

1.1 Global copper industry overview

In the global copper sector, changes in production and consumption patterns and in the restructured composition of international trade flows have been occurring continuously

over the long term. More than 50 countries worldwide participate in copper mining and processing activities, but only six major countries alone account for nearly half of the total production. For example, South America's production volume, which accounted for one-quarter of global output in 1985, had surged to nearly half by 2005. This sharp increase is attributed not to geological reserves but to sustained, large-scale investment in the mining and metallurgical sectors. During this period, global copper production doubled, mainly because of rapid industrialization and infrastructure development programs in developing countries, which sharply increased demand for copper. China has become the world's largest copper consumer due to its industrial expansion, urban development, and ongoing construction activities, underscoring this trend (Crowson, 2012). In line with this, China's imports of copper concentrate have surged sharply since the early 2000s, driven by bilateral trade cooperation and expanded smelting capacity. Chile and Peru form the core of the South America–Asia supply (Nakajima et al., 2018). In the international market, the supply-demand balance for copper concentrate remains extremely sensitive, and even operational errors can trigger significant market reactions. When copper concentrate is in short supply, inventories fall to extremely low levels—sometimes failing to cover even price volatility and fueling speculative trading. Such supply conditions can lead to unplanned operational disruptions, for example, unplanned operational disruptions at the central Escondida plant or strikes at Grupo México's mines caused significant production losses, directly leading to acute short-term shortages and sharp price increases. In contrast, when demand growth slows or short-term production increases outpace consumption, the market quickly reverses into a surplus, which continues to have a substantial impact on systemic operational volatility and broader macroeconomic conditions (Crowson, 2012).

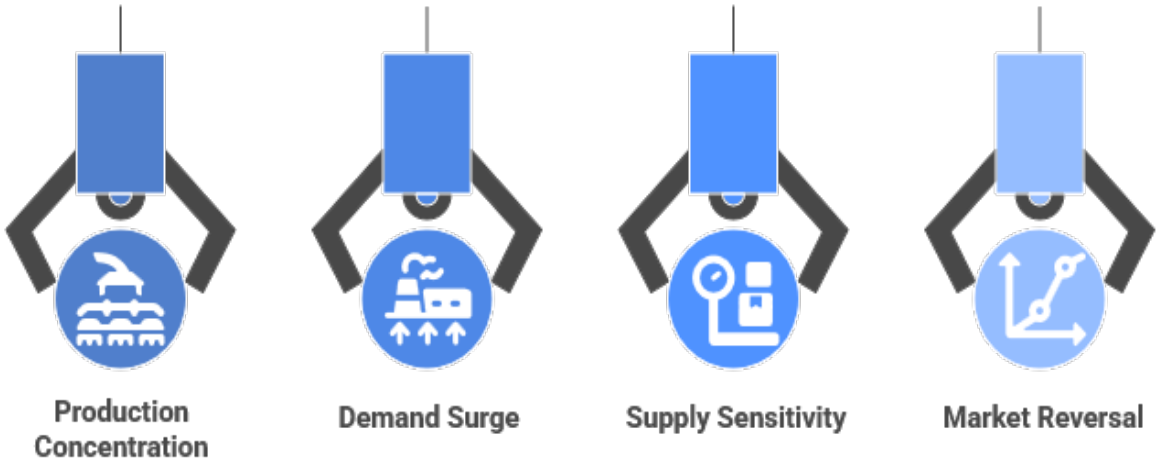


Figure 3. Copper market dynamics

Historically, the world's leading copper producer and, from the late 19th century until after World War II, accounted for more than half of the global market. However, that leading position was maintained for a long time in mining regions that had been in use (for example, Michigan). The ore grade gradually declined, and as higher-grade copper deposits were discovered in other regions, intense competition arose, ultimately reshaping global production (Singer, 2017).

In the current environment of continuously declining ore grades and the weakening competitiveness of primary raw material extraction, ensuring the sustainability of metal resources necessitates a transition toward a circular economy model that prioritizes resource efficiency over a sole reliance on extraction. This paradigm shift is illustrated in the following schematic.

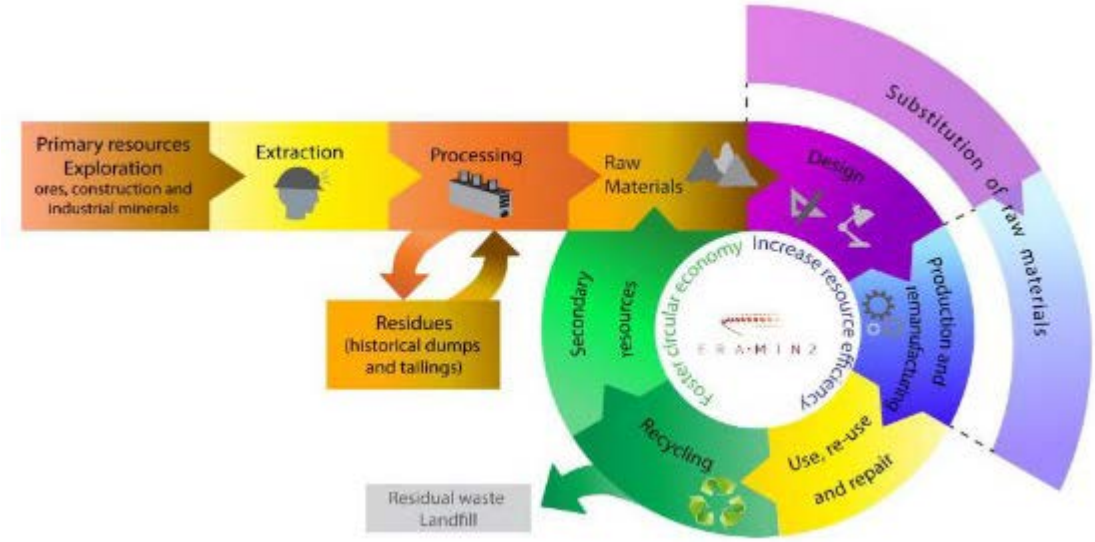


Figure 1. Circular economy concept (https://www.era-min.eu/)

The global copper resource has surpassed approximately one trillion tons, which is significant for the economy. However, technological conditions indicate that long-term supply can remain stable, ore grades are declining in mining regions, so to keep profits steady, production must be significantly increased and processed using advanced methods and technologies. Refining on a large scale using advanced methods and technologies will be required. Moreover, the future demand trend is driven by two conflicting drivers: population growth and GDP growth, both of which are expected to increase copper consumption. (Schipper et al., 2018). The processing technology for copper depends on the mineralization state of the ore, the amount of capital investment in the processing plant, and environmental management, while the long- and short-term requirements for operating a new mine constrain supply. (Clark et al., 2006).

Geopolitical factors continue to significantly impact copper sales in Chile. Free trade agreements between China and other countries are redefining copper concentrate shipping routes and strengthening long-term strategic supply cooperation. At the same time, countries with economies dependent on imports are securing guarantees to forecast future supplies and ensure stable copper availability. Interest is increasingly growing in securing future supplies, ensuring stable copper availability, reducing risks, acquiring mining investments, or entering into long-term purchase agreements (Nakajima et al., 2018).

In comparison, mature markets such as Canada, the US , Japan, Spain, and Italy have per capita demand ranging between 4-9 kgs. However, there are some outliers, such as Germany, China, Turkey, and South Korea, whose per capita income is proportionately higher compared to their GDP per capita. It is expected that South Korea and Japan will shift their production of copper end-use and first-use products to lower-cost regions. Germany has been an exceptional outlier, and it has achieved that through its success in the automotive and engineering industry, including power generation equipment, which are intensive copper-consuming sectors, and therefore its demand per capita is high (IMF, UN Population

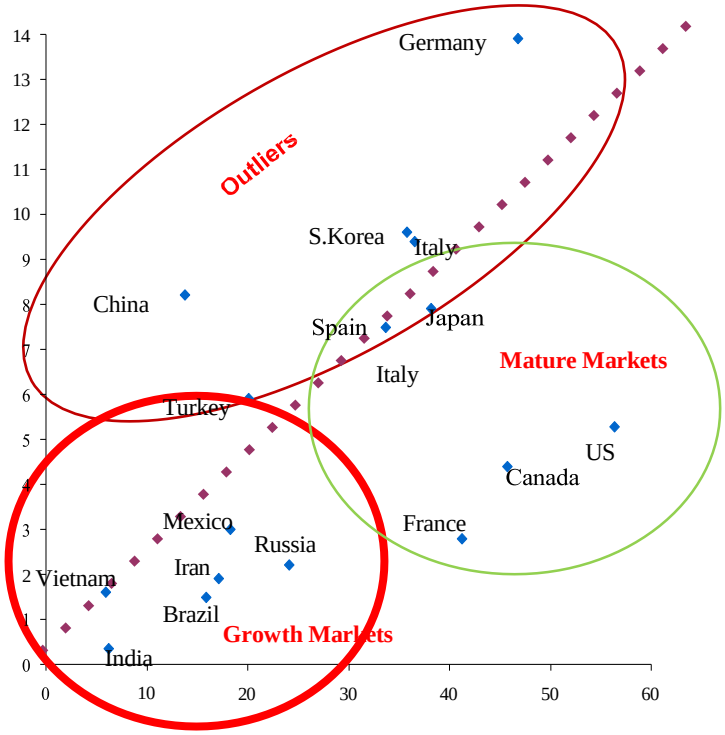


Figure 2. Global copper demand intensity

Refined copper demand is forecast to grow at 1.7% p.a to 2035 from 2018. The total increase in demand during the same period is estimated at 8.2 million tonnes of copper.

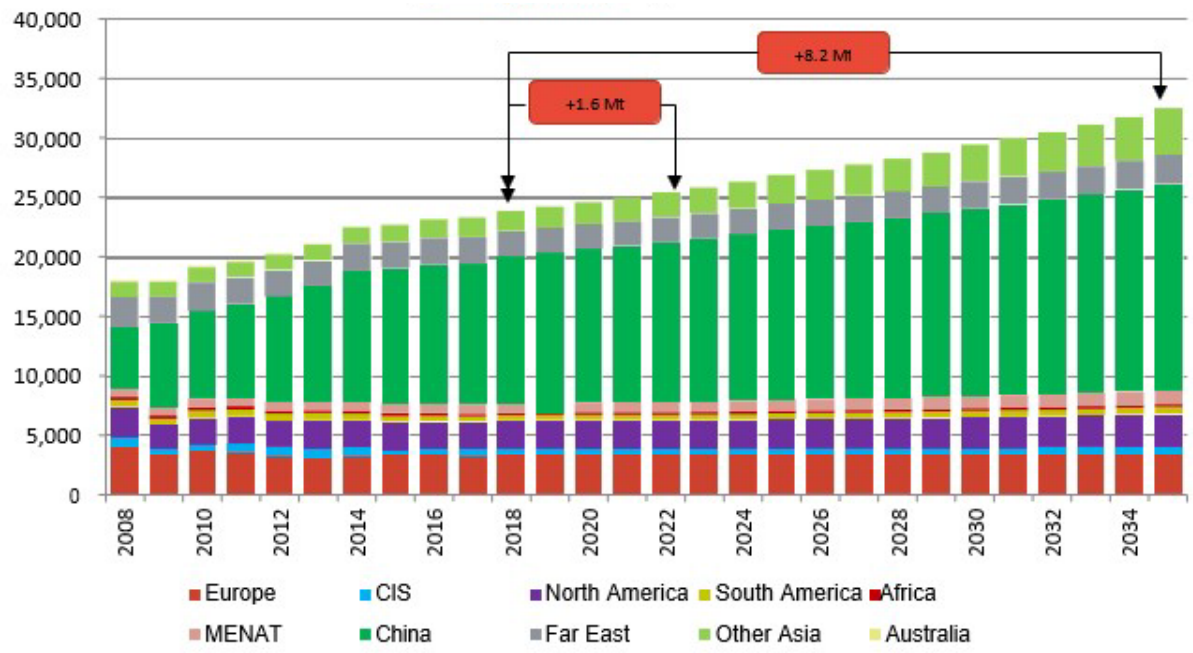


Figure 3. Forecast of refined metal demand, copper metal content (Hatch)

The main difference in the demand outlook compared to historical trends is the heavy promotion of EVs for environmental reasons. A typical EV consumes 60 kg to 83 kg of copper, while an internal combustion engine consumes 23 kg of copper. China will account for 39% global EV market by 2035. This will be a key driver for copper demand growth in this country.

The U.S government increased tariffs on $200 billion worth of Chinese goods from 10% to 25% in May 2019. It is unlikely that these trade disputes will persist indefinitely. We expect the trade relations between China and the US will be restored. However, exports of Chinese goods to the US could decline, and consequently, demand growth for refined metals will be lower than in historical trends.

Demand growth will shift away from China to regions such as India and Southeast Asia, benefiting from growth in construction and infrastructure spending and automotive production. In recent years, resource shortages, breakdowns in mining equipment, and weather-related challenges have created instability in copper prices. At the same time, the industry is being transformed by technological innovation and a wide range of structural factors. Ore grades are also declining. The increasingly complex mineral composition is accelerating the development of advanced technologies, including

efficient leaching processes, selective flotation enrichment techniques, and expanded operations to recycle secondary copper streams. Despite these technological advances, market operations remain complex due to rising demand in Asia and significant fluctuations in the activities and production capacities of major South American producers (Crowson, 2012).

1.2 Copper concentrate sources and mineralogy

Copper concentrate is a key raw material in global copper production, and the processing technology is determined by the deposit's geological structure and the various mineralogical characteristics of its minerals. Porphyry deposits with high ore-mineralization volumes but low to medium ore grades and polymetallic zonation; large-scale, finely grained, volcanic-hosted polymetallic sulfide (VMS) deposits, as well as copper deposits with layered structures hosted in sedimentary strata; and large deposits containing various Cu–Pb–Zn sulfide ratios and associated metals (Franklin et al., n.d.). Ore grade forms a concentration with its own unique mineralogical composition, accompanying gangue minerals, and contamination profile, and these characteristics influence metal recovery in the beneficiation process, flotation selectivity, smelting and leaching mechanisms, as well as the stable operation and product quality of subsequent refining stages.

1.2.1 Porphyry Deposits

Porphyry copper deposits account for most of the world's copper supply and consist of relatively uniform mineral assemblages dominated by chalcopyrite, bornite, and chalcocite, with the rock matrix typically composed of quartz–sericite (phyllic) alteration minerals. These deposits are characterized by continuous, wide-area distribution and controlled, fine, network-like mineralization along fractures, creating favorable conditions for open-pit mining. The first hypogene copper content is typically 0.3–1%, and when a supergene enrichment crust forms over the hypogene zones, secondary chalcocite and covellite develop in the well-permeable, pyrite-rich strata, raising the copper content to 1–3% (Sillitoe, 2010). The mineral composition of porphyry copper ore is relatively simple, enabling a straightforward flotation scheme. However, when factors such as alteration zoning patterns and clay mineral content change, additional operational adjustments—such as revising reagent settings become necessary(Srdjan M. Bulatovic, n.d.).

A primary driver behind the secular decline in average ore grades is the structural shift in the genetic types of deposits being exploited. From the 19th century through the mid-20th century, a substantial portion of global copper production was derived from massive sulphides, copper skarns, polymetallic veins, and sediment-hosted copper deposits. However, with the depletion of output in Africa, Western Europe, and Eastern Canada, the relative share of these deposits has diminished. While certain strategic deposits, such as those in Poland, remain significant, and Central African production is undergoing a revival, the dominant share of copper production has shifted toward porphyry deposits. The inherent variations in geological structure and mineralization across different deposit types are fundamentally reflected in the divergent average yields observed across different countries and mining regions (Crowson, 2012).

Table 1. Copper deposit types (Crowson, 2012)

№	Type of ores	Number of deposits	Cu content lowest,%	Cu content, median,%	Cu content, high,%
1	Porphyry copper	208	0.31	0.54	0.94
2	Sediment-hosted	57	1	2.1	4.5
3	Cu skarn	64	0.7	1.7	4
4	Polymetallic replacement	52	n.a	0.094	0.87
5	Polymetallic veins	75	n.a	n.a	0.89
6	Cyprus massive sulphides	49	0.63	1.7	3.9
7	Besshi massive sulphides	44	0.64	1.5	3.3
7	Kuroko massive sulphides	432	0.45	1.3	3.5
8	Synorganic-synvolcanic ni-cu	32	0.13	0.47	1.3

A primary driver behind the secular decline in average ore grades is the structural shift in the genetic types of deposits being exploited. From the 19th century through the mid-20th century, a substantial portion of global copper production was derived from massive sulphides, copper skarns, polymetallic veins, and sediment-hosted copper deposits. However, with the depletion of output in Africa, Western Europe, and Eastern Canada, the relative share of these deposits has diminished. While certain strategic

deposits, such as those in Poland, maintain their significance and Central African production undergoes a revival, the dominant share of copper production has transitioned toward porphyry deposits. The inherent variations in geological structure and mineralization across different deposit types are fundamentally reflected in the divergent average yields observed across different countries and mining regions. (Crowson, 2012)

1.2.2 Volcanogenic massive sulfide (VMS) and Polymetallic massive sulfides

VMS-derived deposits have more complex, diverse mineral compositions. The mixture of minerals—chalcopyrite, sphalerite, galena, pyrite, and in smaller quantities, tennantite or sulphosaltz—is processed by flotation technology that demands highly refined operational techniques. The geometry of the deposit and the zoned distribution of metals further complicate mine planning and processing. (Sillitoe, 2010).

Ores extracted from such deposits typically contain high concentrations of co-occurring metals. They can be economically profitable in favorable market cycles but require strict control when pollution levels exceed the requirements of copper smelting plants. Large-scale Cu–Pb–Zn sulphide deposits are more heterogeneous in terms of mineral composition and structural organization. (Qicheng Feng and Guang Han, n.d.). Depending on the ore's structural framework and the degree of relaxation, it is necessary to optimize the grain size. The deposits are partially oxidized or pyrrhotite-dominated, which affects reagent selection and processing operations. In deposits containing coral-shaped pyrite, the high Co/Ni ratio enables the production of valuable by-products, but the cobalt-enrichment characteristics create complications.

1.2.3 Mineralogy-Driven Metallurgical Behaviors

Mineralogy is an important factor in optimizing the flotation process and enrichment scheme. When processing sulphide ores, iron-suppressing inhibitor reagents are commonly used to prevent adverse effects on chalcopyrite flotation. Microstructural studies have shown that pyrite surfaces are coated with a copper layer or co-enriched with sulphosalt and bismuth impurities within chalcopyrite grains, thereby reducing the efficiency of collector reagents and altering selectivity. In copper ores with a high pyrite content (for example, Alumbrera and OK-Tedi), it may occur in a free form or be trapped within pyrite. Therefore, in the smelting process, to fully process the copper concentrate and to maintain the balance between the value of the by-products and the primary

metal, it is essential to employ specific collector reagents and modified technological schemes. (Srdjan M. Bulatovic, n.d.).

1.2.4 Hydrometallurgical issues

The mineral's structure and composition also influence the leaching process. The dissolution of ferric sulphate supported by the addition of pyrite exhibits high efficiency in dissolving chalcopyrite when the pyrite-to-copper-sulphide ratio is on average 2:1. The process temperature is critical. The condition for efficient dissolution occurs at approximately 85 °C, whereas redox conditions form a passivation layer that significantly slows the reaction rate (Koleini et al., 2011).

Secondary sulphides, such as chalcocite and covellite, undergo a reaction suitable for chloride-based leaching systems, for example, CuproChlor®. This system enhances permeability during agglomeration by using calcium chloride and sulphuric acid, creating a chloride-rich microenvironment that is favorable for sulphide dissolution. (Cerda et al., 2017). These systems are not complex to smelt and yield good results in the further processing of secondary sulfide-dominant concentrations.

1.3 Objective of the thesis

Erdenet Mining Corporation was selected as the project site due to its strategic importance as Mongolia’s largest copper–molybdenum producer, contributing more than half of the nation’s overall output and serving as a central pillar of the country’s mining economy. With over four decades of continuous operation on a complex porphyry Cu–Mo ore system, the plant provides extensive operational data and a robust industrial platform for evaluating technological innovation, processing efficiency, and metallurgical performance. Furthermore, any advancements or improvements developed through this project have direct potential to enhance national-level mining sustainability and metal recovery, making Erdenet an ideal and high-impact subject for applied research.

1.3.1 District-Scale Geological Setting

The Erdenetiin-Ovoo copper–molybdenum deposit cluster is situated within the Erdenet Cu–Mo metallogenic district, which lies in the Bayan Gol continental margin arc terrane of the Northern Mongolian super terrane, corresponding to sheet M-48-XXVII. This ore cluster belongs to the Erdenet ore district [Cu, Mo (Ag, W)], specifically within the

Erdenet ore [Cu, Mo (Ag, W)]. The Erdenet and Züül River ore knots form a unified structural–metallogenic body occupying the western half of the 1:200,000-scale M-48-XXVII map sheet. Within the Erdenet ore knot, the Erdenetiin-Ovoo Cu–Mo deposit cluster—comprising the Western-North, Central, and Oyut zones—is located, along with several satellite prospects including Turmalin, Chuluut, Deed Nariin Gol, and Tsagaan Chuluut. The Züül River ore knot, located southwest of the Chuluut and Deed Nariin Gol prospects, hosts the Shand ore area, which includes the Shand, North Shand, South Shand, and East Shand prospects. The Orkhon–Selenge composite basin is bordered to the north by the Khuvsgul Range continental margin arc terrane and to the south by the Khangai–Khentii uplift. Regionally, the basin is an approximately 400-km × 160–200-km elongate structural depression extending predominantly in an east–west orientation. The Carboniferous–Permian stratigraphy and lithology that constitute the late Paleozoic composite structures of the Bayan Gol terrane were previously investigated in detail by V. V. Kepezhinskas and I. V. Luchitskii (1973), M. V. Durante (1976), A. A. Mossakovskii and O. Tömörtogoo (1976), *Lower Cambrian and Carboniferous Biostratigraphy of Mongolia* (1980), and A. T. Matrenitskii et al. (1980, 1983). A 1:200,000-scale geological map of the district is presented in Figure 4.

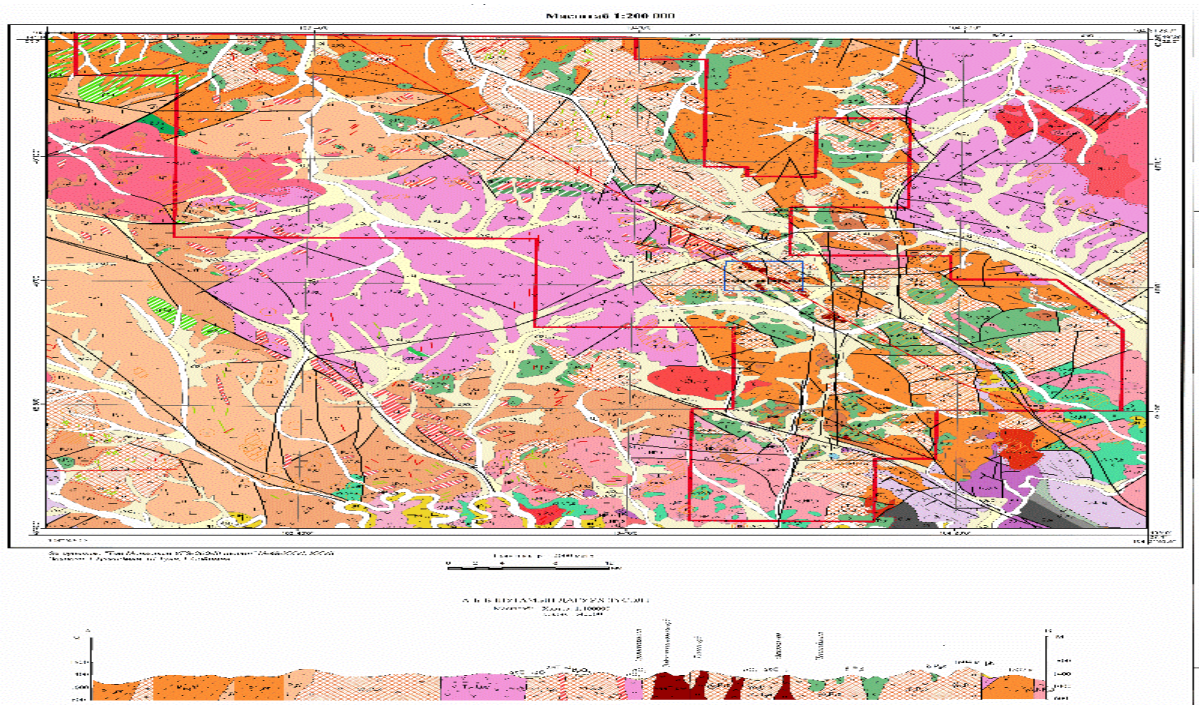


Figure 4. District Geological Map

The basement of the Orkhon–Selenge depression consists of the Lower–Middle Neoproterozoic Darkhan Formation, which comprises gneiss, marbled limestone, crystalline schist, quartz–syenite–chlorite schist, greenschist, and sparsely distributed coeval quartz diorite intrusions that cut these units.In contrast, the Late Paleozoic Orkhon–Selenge superimposed basin comprises Devonian undifferentiated sedimentary rocks; terrigenous deposits of the Lower Carboniferous Urmügtei Formation and the Lower–Upper Carboniferous Arteil Formation; volcanogenic rocks of the Lower–Middle Permian Khanūi Group; volcanogenic–sedimentary sequences of the Middle–Upper Triassic Avzaga Formation; Upper Triassic–Lower Jurassic Mogod Formation; and Miocene basaltic rocks of the Chingel Formation. (*EMC, Technological Instruction*, 2024).

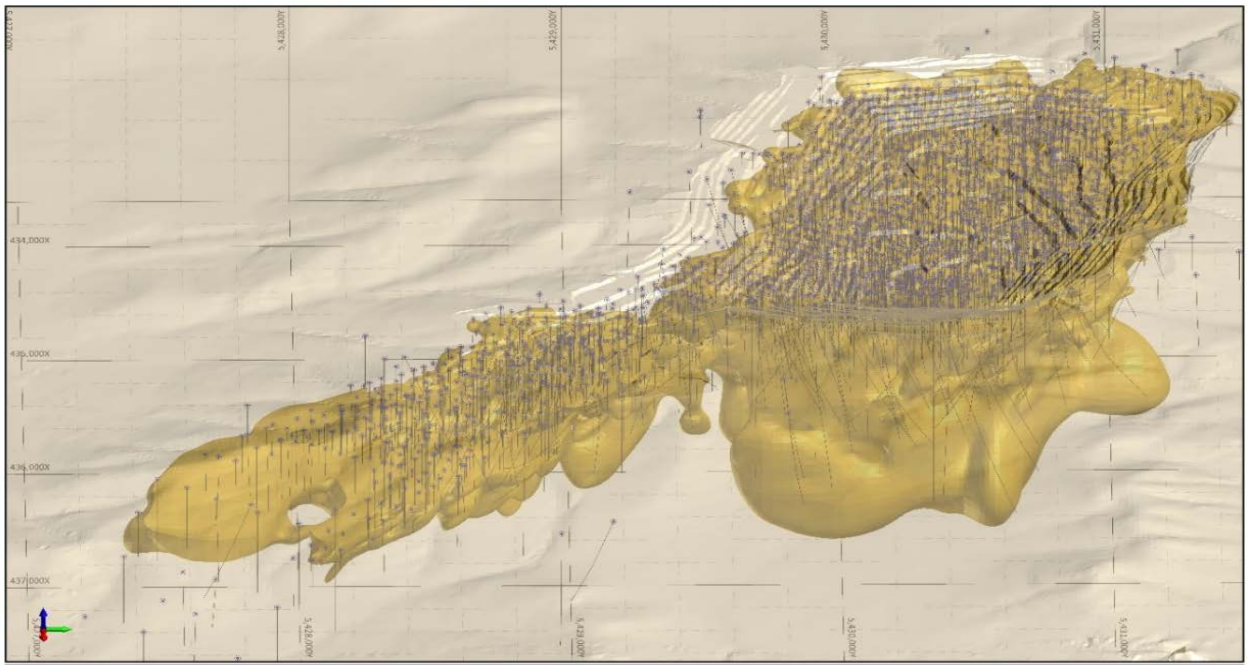


Figure 4. Erdenetiin ovoo deposit ore body

1.3.2 Leached and oxidation zones

The oxidation zone is predominantly distributed along the deposit's central fault line, extending into the southeastern and western sectors. The thickness of this zone typically fluctuates between 60–80 meters from the surface, reaching depths of 150–170 meters along the central fault. This zone is characterized by rocks that have

undergone significant weathering and hydrothermal alterations, specifically kaolinization, sericitization, and silicification. Secondary ore minerals are observed as irregular coatings within the host rock, while primary minerals occur rarely as relicts. Structural features such as veins, fractures, and shear zones provide a favorable environment for the development and maturation of the oxidation zone.

The primary characteristics of the leaching zone (leached cap) include:

- Copper depletion: Due to the dissolution and migration of copper minerals, average grades decrease to approximately 0.1%.
- Oxidized mineral assembly: Approximately half of the ore minerals have transitioned into phosphates, carbonates, silicates, and native copper.
- Sulfur depletion: Sulfur content is low (<0.2%), with pyrite comprising less than 0.1% of the mineral composition.

Mineral Composition of the Leached and Oxidation Zones:

- **Major Minerals:** Limonite, jarosite, pyrite, hematite, chrysocolla, turquoise, brochantite, malachite, azurite, magnetite, and manganese oxides.
- **Minor/Accessory Minerals:** Chalcocite, chalcopyrite, and ferrimolybdite; rarely covellite, molybdenite, pyrrhotite, bornite, and fahlore.

Detailed mineral descriptions:

- **Native Copper:** Occurs as grains, fine veinlets, and coatings, ranging from sub-millimeters to several centimeters in size. It is frequently associated with cuprite, which in turn occurs with tenorite and delafossite.
- **Cuprite:** A dominant mineral in mixed ores, appearing as cryptocrystalline or earthy masses in shades of brown and brownish red. It typically coexists with tenorite, delafossite, malachite, and azurite.
- **Tenorite:** Found as black to dark grey, fine-grained, thin scales or earthy aggregates, closely associated with cuprite, chalcocite, and hydrous iron oxides.
- **Delafossite:** Forms tabular or disc-like crystals varying in size, occasionally reaching 2 cm. It often forms spherulitic aggregates and is typically associated with cuprite, tenorite, native copper, and hematite.
- **Malachite:** Occurs as coatings, crusts, and films along fractures, and rarely as vugs/nests. It is found in association with azurite, cuprite, and tenorite, as well as sulfides like chalcopyrite, chalcocite, and bornite.

- **Azurite:** Similar in origin and form to malachite, often occurring as hard films associated with malachite and goethite.
- **Chrysocolla:** Appears as botryoidal or small granular grains, forming intergrowths with malachite, azurite, and brochantite.
- **Turquoise:** Occurs as dense, massive veins or occasionally as nests, with vein thicknesses ranging from millimeters to several centimeters.
- **Brochantite:** Found as coatings or powdery masses, sometimes filling rock fractures.
- **Antlerite:** Occurs as small crystals in quartz veins alongside pyrite and bornite.
- **Chalcanthite:** A water-soluble mineral occurring with other hydrous copper and iron sulfates.

Sulfides (chalcopyrite, chalcocite, covellite, bornite, molybdenite, and pyrite) serve an accessory role within the oxidized and mixed ore compositions. In the oxidized ore, molybdenum mineralization is primarily represented by ferrimolybdite, appearing as yellow, powdery limonite-like aggregates which eventually transition into goethite.

The final oxidation product of iron-bearing sulfides is goethite, which occurs as veinlets filling open spaces. Additionally, jarosite is found as films, coatings, and occasionally as yellowish-brown friable soil-like masses.

Textures and Structures:

The mineral structures in oxidized and mixed ores are diverse, including:

- **Colloform/Metallic:** Limonite, tenorite, chrysocolla, turquoise, jarosite.
- **Radiating:** Malachite, azurite, brochantite.
- **Replacement and Clastic:** Chalcocite, covellite, bornite.
- **Exsolution:** Chalcopyrite.
- **Foliated/Scaly:** Molybdenite.

Table 2.Mineral Composition by Enrichment Zones

№	Minerals name	Primary	Secondary	Oxidized
1	Chalcopyrite	1.10	0.59	0.28
2	Enargite-Tennantite	0.08	0.07	0.01
3	Bornite	0.07	0.09	0.04
4	Chalcocite	0.04	0.23	0.06
5	Covellite	0.03	0.07	0.10
6	Oxidized copper minerals	0.05	0.12	0.41
7	Molybdenite	0.03	0.02	0.01

8	Pyrite	3.70	3.13	2.60
9	Hematite	0.09	0.12	0.59
10	Sphalerite	0.10	0.05	0.07
11	Quartz	33.20	31.22	29.27
12	Plagioclase	23.78	30.60	36.03
13	K-feldspar (Potassium feldspar)	7.01	7.04	10.09
14	Muscovite	23.40	19.55	12.83
15	Clay minerals	4.91	4.91	6.34
16	Carbonate minerals	1.39	1.31	0.31
17	Other minerals	1.02	0.89	0.97

The primary ore minerals within the secondary sulfide enrichment zone are dominated by chalcocite, covellite, chalcopyrite, and pyrite. The associated (accessory) mineral assemblage consists of bornite, fahlore (tetrahedrite-tennantite), oxidized copper minerals, molybdenite, sphalerite, galena, and other minor minerals.

1.3.3 Supergene (Secondary) Sulfide Enrichment Zone

This zone spans across the deposit footprint. The vertical thickness varies significantly, ranging from 10 meters at the periphery to 250–300 meters in the central portion. Since the commencement of mining, the average thickness of the secondary ore zone is estimated at 136 meters.

The boundary between primary and secondary enrichment zones generally lies between the 1280–1310 m levels. In the southern, northeastern, and northern sectors, this interface tends to rise to elevations of 1340–1400 m. The supergene zone is characterized by a complex of silicified and sericitized porphyritic rocks (granodiorite porphyry, dacite, plagioporphyry) and host granodiorites. These are associated with sericite-feldspar-quartz metasomatite zones and quartz-sulfide mineralization, presenting as grey to bluish-grey ores.

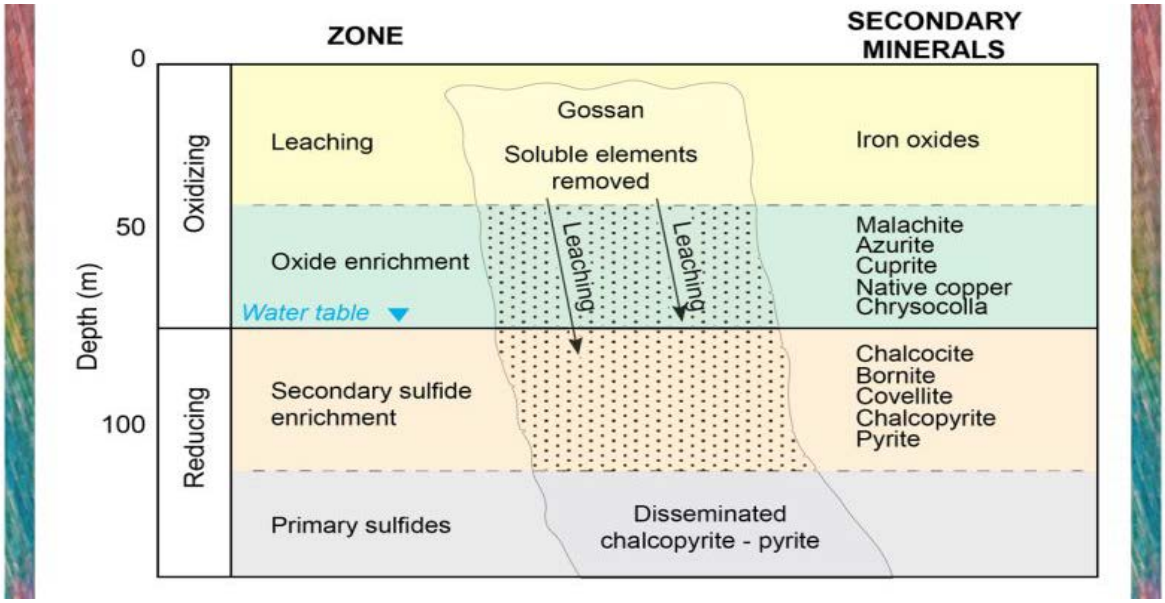


Figure 5. Supergene enrichment (Levinson,1980)

1.3.4 Mineral processing stage

The primary objective of grinding is to prepare finely crushed ore in accordance with the concentrator's design capacity for all stages of mineral processing, while ensuring adequate mineral liberation in the beneficiation products.

The optimal operating conditions of the grinding mills, classifiers, and auxiliary equipment in the grinding section are regulated by a technological operating regime card established based on experimental and research results.

The size and composition of the grinding media charged to the mill are determined experimentally based on ore hardness, primary feed size, maximum particle size, size fraction distribution, throughput, and required degree of grinding.

During long-term operation, steel ball consumption becomes self-balancing; therefore, return spirals are installed at the mill discharge, and no special classification of worn grinding media is required.

In the grinding circuit, variations in primary feed rate, particle size distribution, and slurry density must not exceed ±5% of the values specified in the technological operating regime card.

The Erdenet Concentrator uses a conventional bulk flotation flowsheet to process copper–molybdenum ores. The flotation process consists of the following main processing stages. The following figure shows the general technology schema.

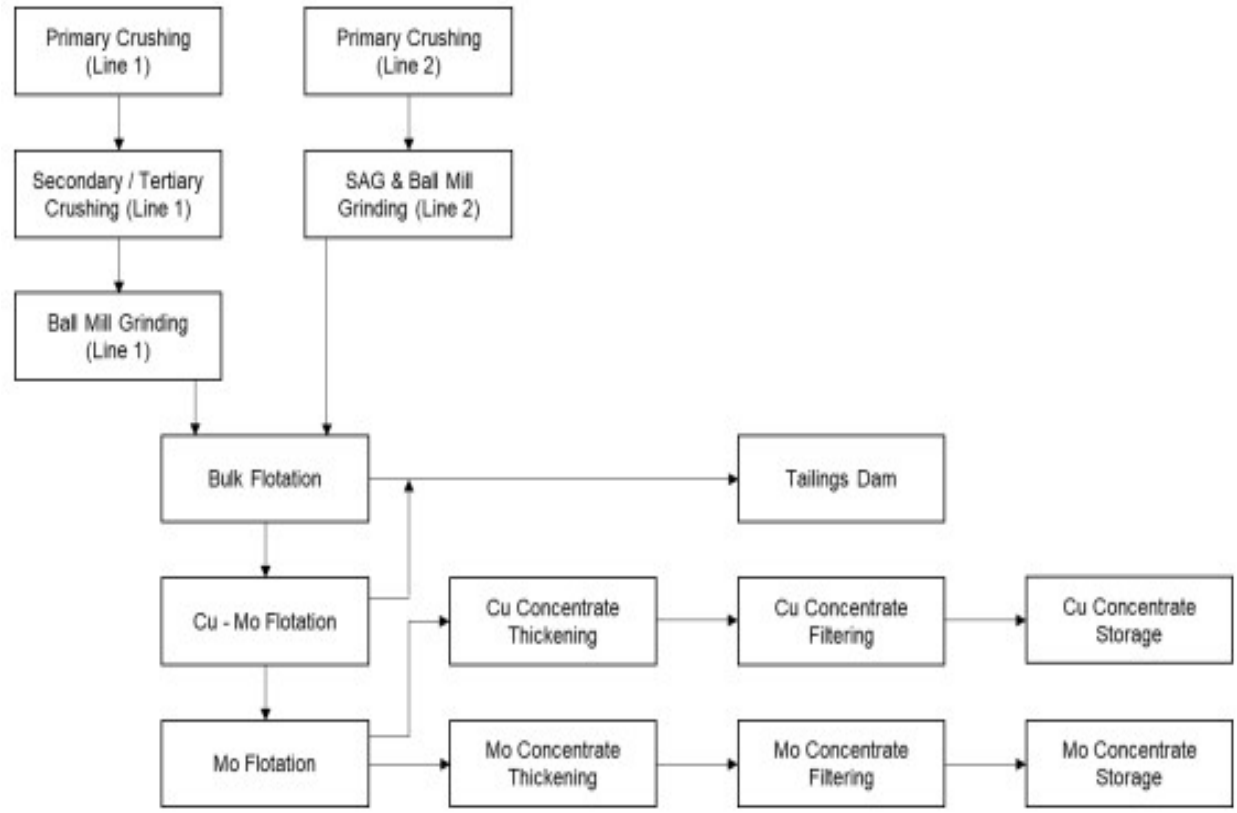


Figure 6. EMC general technology schema

Investigation into the processing flow at the Erdenet Concentrator reveals that the comminution stage serves as the fundamental driver of final recovery outcomes. The strategic utilization of parallel SAG and ball milling circuits is essential for securing the precise degree of mineral liberation required to optimize the particle size profile.

From an operational research standpoint, strict adherence to a 5% tolerance for both primary feed rates and slurry density is paramount. Any significant deviation in these parameters tends to disrupt the equilibrium of the technological regime, directly jeopardizing the efficiency of downstream bulk and selective flotation circuits.

Following the successful separation of values through copper-molybdenum differential flotation, the resulting concentrates undergo a rigorous dewatering process via thickening and filtration. The cycle concludes as the final rejects are channeled to the tailings storage facility. Ultimately, managing the synergy between these complex technological stages remains the cornerstone of maximizing the plant's overall economic and metallurgical performance.

Major challenges:

In recent years, the progressive deepening of mining operations has resulted in increased ore hardness, which in turn has significantly raised the costs of comminution and ore preparation. Concurrently, a continuous decline in the primary copper grade of the ore has been observed. Under these conditions, maintaining and improving production efficiency necessitates an unavoidable increase in mining and processing throughput.

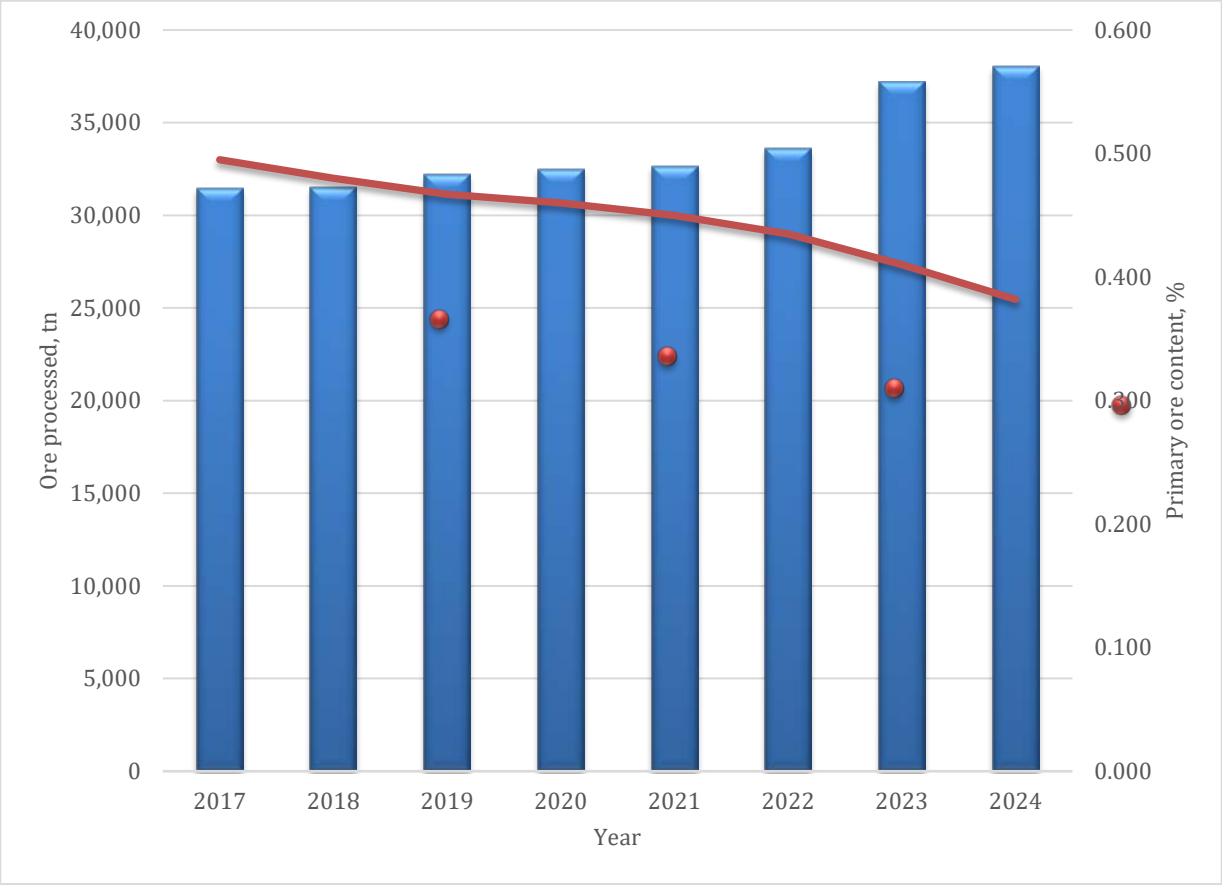


Figure 7. EMC Ore Throughput and Primary Copper Gradeer content

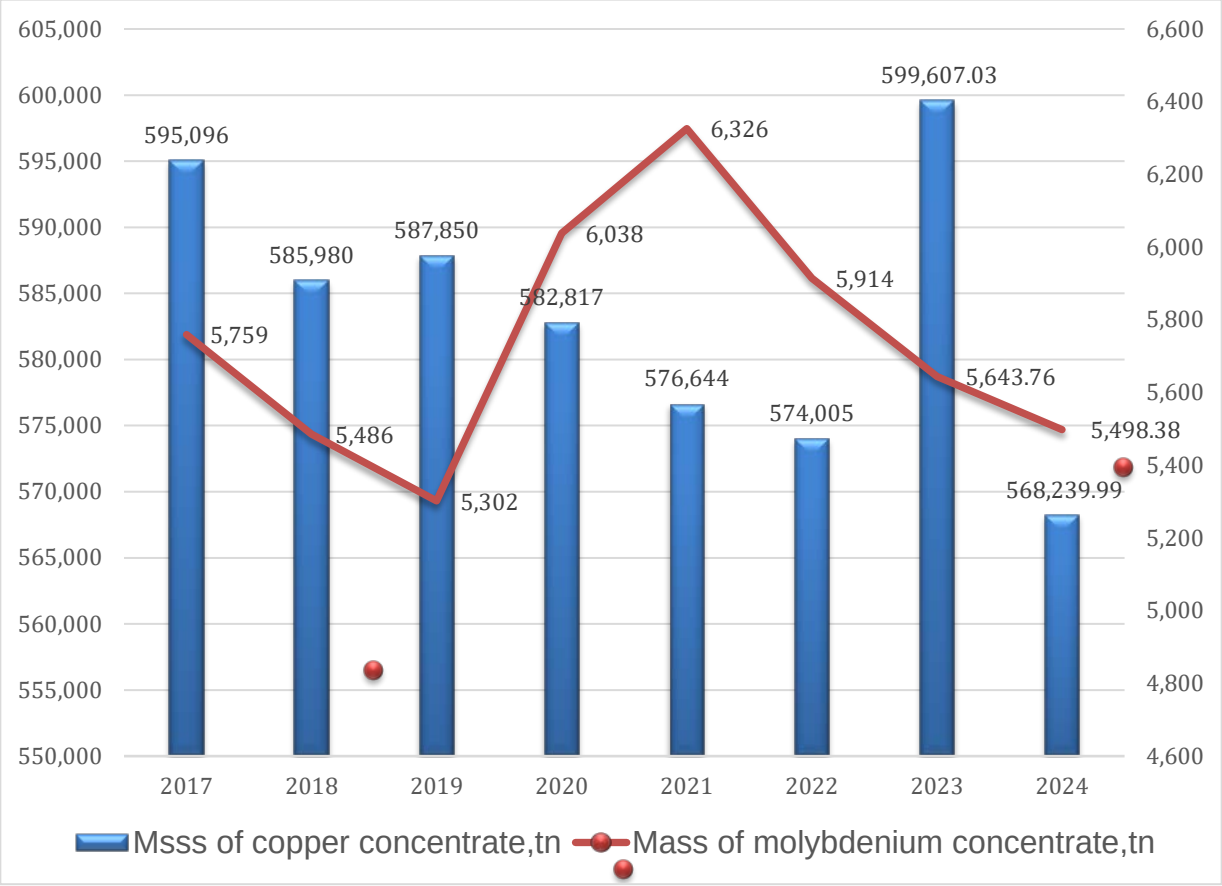


Figure 8. Mass of copper concentrate and molybdenum concentrate

The yield of copper concentrate is inherently subject to fluctuations driven by dynamic geological conditions, reagent efficiency, and operational variables. Given the increasing complexity of ore mineralogy, there is a critical necessity to adopt advanced processing technologies that enhance economic returns. This research evaluates viable strategies for the transition to final product extraction, focusing on maximizing recovery and profitability while adhering to stringent environmental sustainability standards.

1.4 Structure of the Thesis

This thesis is structured as follows:

Chapter 2: Literature Review – Discuss previous research on chalcopyrite and bornite leaching, including chemical mechanisms and process advancements.

Chapter 3: Methodology – Describes the experimental setup, materials used, and analytical techniques for leaching studies.

Chapter 4: Results and Discussion – Presents experimental data on metal dissolution and analysis of leaching behavior.

Chapter 5: Economic Evaluation

Conclusion – Summarizes findings and suggests potential improvements for industrial applications.

Through this study, a comprehensive understanding of the leaching behavior of chalcopyrite and bornite will be achieved, supporting the development of more efficient extraction technologies for copper concentrate.

CHAPTER 2. LITERATURE REVIEW

2.1 Introduction

Copper ore is one of the world's most important industrial raw materials, and chalcopyrite and molybdenite in particular are of major economic significance. Despite decades of technological advances in mineral processing and extractive metallurgy, hydrometallurgical methods for efficiently processing concentrates remain problematic due to the inherent characteristics of primary copper sulfides and the minerals contained within the concentrate structure. Between them remains unresolved to this day (Fuerstenau & Han, 2009) . When processing chalcopyrite-dominant copper concentrate by conventional methods, pyrometallurgical smelting, refining, and assaying techniques are widely used. Using this method increases sulfur dioxide emissions and complicates the processing of low-grade, highly contaminated ore (Schlesinger, 2011). When processing chalcopyrite-dominant copper concentrate by conventional methods, pyrometallurgical smelting, refining, and assaying techniques are widely used. Using this method increases sulfur dioxide emissions and makes processing low-grade ore challenging (Schlesinger, 2011).

Hydrometallurgical processing has emerged as a supplementary or alternative method, offering advantages at low temperatures, improved metal selectivity, and greater suitability for processing low-grade ores. However, leaching chalcopyrite-rich concentrates is very slow and inefficient due to kinetic limitations and surface passivation phenomena. Borite-rich concentrates generally dissolve well; however, their dissolution depends heavily on their composition and on the chemical composition

of the sulfide phases and the leaching solution. (Fuerstenau & Han, 2009; Ruiz et al., 2015).

Molybdenite (MoS_2) occurs in copper ore as layered sheets, with a layered hexagonal crystal structure and strong covalent Mo–S bonds. The –S bond renders molybdenite chemically inert under most acid copper leaching conditions, so it generally remains unchanged during copper leaching. This natural selectivity has long been exploited in industry. (Fuerstenau & Han, 2009; Patnaik, 2003). However, the state of molybdenite influences electrochemical and galvanic interactions in the slurry, intricately altering the chalcopyrite dissolution process.

The main limitation of the leaching system is the formation of a passivation layer on the chalcopyrite grains, typically consisting of elemental sulfur, jarosite-type iron sulfate, and iron oxyhydroxide. These layers impede electron transfer and mass transport, reduce dissolution rates, and prevent complete copper dissolution (Chalcopyrite Dissolution in Cupric Chloride Media, 2012).

To overcome these limitations, it is necessary to introduce Other types of oxidants that can improve the process, disrupt the passivation layer, or prevent its formation (Lundström, n.d.). As a result, advanced oxidative leaching strategies employing iron-based systems, chloride-assisted leaching, iodine/iodide redox systems, and potent oxidizing agents such as ammonium persulfate have attracted considerable research attention. (Schlesinger, 2011).

This section includes information on the mineralogical characteristics of chalcopyrite, bornite, and molybdenite in copper ore, their structure–reaction relationships, and the hydrometallurgical challenges associated with them. It highlights the fundamental mechanisms of sulphide leaching and passivation, as well as the advanced oxidation leaching systems developed to overcome these obstacles. The concepts outlined above form the scientific basis for the experimental leaching strategies investigated in the following chapters of this master's thesis.

2.2. Surface passivation mechanisms in chalcopyrite leaching

Surface passivation is the main kinetic limitation in the hydrometallurgical leaching of copper-rich chalcopyrite. Although thermodynamically favorable oxidation pathways exist, under atmospheric conditions, the dissolution of chalcopyrite is often hindered by electron-transfer limitations and delayed by the formation of a reaction layer that

restricts mass transfer between the mineral surface and the leaching solution (Fuerstenau & Han, 2009)

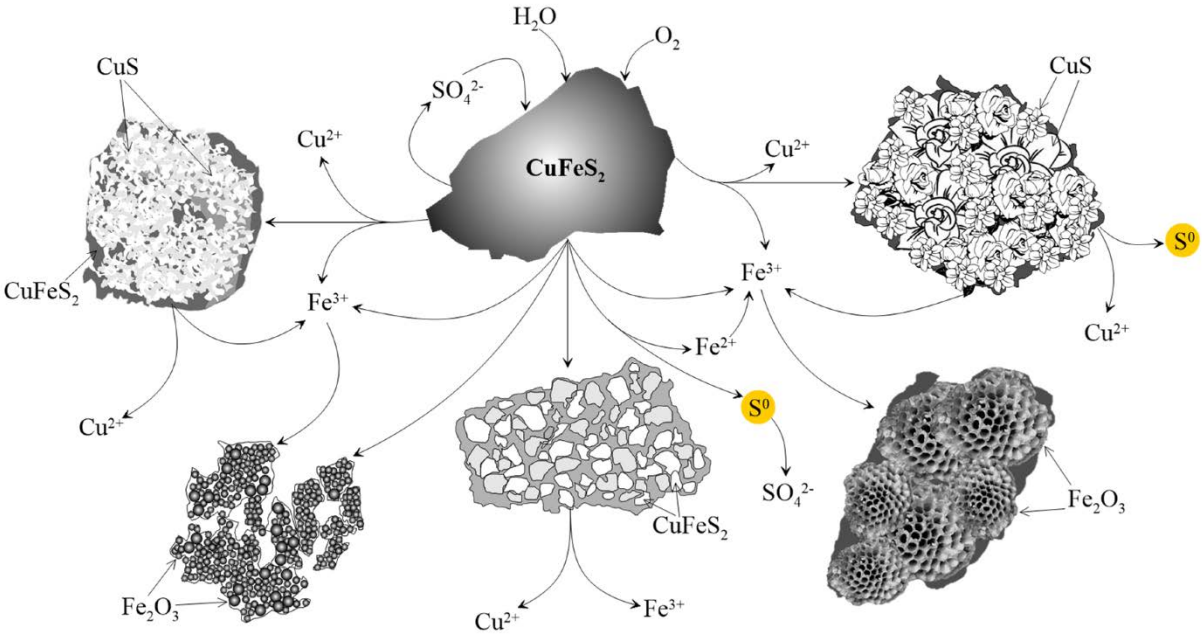


Figure 9. The proposed dissolution and passivation mechanisms of the chalcopyrite leaching system (Jiang, L., Leng, H., & Han, B., 2023)

During the leaching process, elemental sulfur (S^0) and iron sulfate precipitates, such as jarosite, develop on the mineral surface. As illustrated in the figure, this dense passivation layer acts as a physical barrier that restricts the access of reagents to the mineral interface, ultimately inhibiting the dissolution process.

Key passivation mechanisms include:

- **Elemental Sulfur (S^0) Layer Formation:** The oxidation of sulfide sulfur often yields a dense, electrically insulating layer of S^0. This layer physically impedes the transfer of lixiviant species, resulting in reduced leaching rates.(Chmielewski & Kaleta, n.d.) The oxidative dissolution of sulfide minerals, particularly chalcopyrite, is frequently hindered by the formation of a tenacious, electrically insulating layer of elemental sulfur () on the mineral surface (Chmielewski & Kaleta, n.d.). This passivation layer acts as a physical diffusion barrier, significantly impeding the mass transfer of lixiviant species to the unreacted mineral core, which consequently leads to a drastic reduction in leaching kinetics (Dutrizac,1990). Advanced surface characterization studies indicate that this phenomenon is not exclusively attributed to formation. Notably, Klauber et al. (2001) demonstrated that the accumulation of metastable, metal-deficient polysulfide species

on the mineral-solution interface creates a significant barrier to electron transfer, further exacerbating the passivator effect.

- **Secondary iron-bearing precipitates and surface passivation**

Iron ions released during the dissolution process, particularly at moderate pH values, can reprecipitate as ferric hydroxides or basic sulfates, forming a tenacious film over the chalcopyrite surface.(Oxdizationstep, n.d.) In addition to the formation of elemental sulfur, the mobilization of iron ions during the oxidative dissolution of chalcopyrite presents a significant challenge to leach efficiency. As iron is released into the solution, particularly under conditions of moderate pH (typically pH > 2.0), the solubility of ferric species () decreases, leading to the spontaneous reprecipitation of secondary mineral phases (Oxdization step, n.d.). These precipitates primarily manifest as amorphous ferric hydroxides () or crystalline basic ferric sulfates, commonly referred to as jarosite (Cordoba et al., 2008).

- **The Impact on Mass Transfer and Kinetics**

Unlike the sulfur layer, which is often porous in its early stages, iron-bearing precipitates can form a remarkably tenacious and coherent film over the mineral interface. This secondary coating serves as a robust physical barrier that isolates the chalcopyrite surface from the bulk lixiviant, effectively arresting the transport of both reactants and products (Zhu et al., 2011). Furthermore, the thermodynamic stability of these iron films—especially jarosite—makes them particularly difficult to remove without significant adjustments to the solution chemistry, such as lowering the pH or increasing the concentration of complexing agents (Tosun et al., 2012).

The accumulation of these precipitates not only inhibits ionic diffusion but also disrupts the electrochemical potential at the mineral-solution interface, causing a premature cessation of the leaching reaction, even when significant amounts of unreacted mineral remain (Crundwell, 2013)

- **Electrochemical and chemical influence of accessory sulfides**

Research suggests the formation of an intermediate, non-stoichiometric copper-deficient sulfide layer (e.g., $Cu_{1-x}FeS_2$ or CuS_2) on the chalcopyrite surface due to the incomplete oxidation of the sulfide lattice. This highly resistive layer kinetically stabilizes the surface against further oxidative attack.

Pyrite is electrochemically active and influences the redox speciation of iron (Fe^{2+}/Fe^{3+}) in the aqueous environment. While the ferric ion (Fe^{3+}) is a primary oxidant for chalcopyrite, high concentrations can exacerbate iron precipitation and subsequent passivation. Pyrite can also participate in galvanic interactions with chalcopyrite, though the net effect on dissolution kinetics is complex and context dependent. Most abundant associated mineral and exerts a profound influence on the redox environment. Due to its high rest potential (approximately vs. SHE), pyrite typically acts as a cathode when in physical contact with chalcopyrite (vs. SHE), which becomes the anode (Mehta & Murr, 1983). This galvanic couple accelerates the anodic oxidation of chalcopyrite, theoretically enhancing copper recovery. However, the increased release of iron species can be counterproductive; elevated concentrations of ferric ions (Fe^{3+}) in the boundary layer often trigger the rapid precipitation of jarosite and other basic ferric sulfates, leading to the secondary passivation described previously (Abraitis et al., 2004).

Molybdenite (MoS_2) and Surface Interactions: Molybdenite is generally considered chemically inert under typical leaching conditions. However, its presence can influence the electrochemistry of the slurry and surface interactions, potentially affecting the overall dissolution rate of chalcopyrite through subtle galvanic effects or surface coating phenomena. To further illustrate the complexity of these interactions, the table below provides a detailed breakdown of the galvanic and chemical influences of common sulfide minerals. In contrast to pyrite, molybdenite is characterized by its relative chemical inertness under conventional atmospheric or bio-leaching conditions. Despite its stability, it contributes to the slurry's electrochemical profile. Its layered crystalline structure and high rest potential (ranging from to) allow it to participate in subtle galvanic interactions (Holmes & Crundwell, 2000). Furthermore, molybdenite can act as a physical masking agent; its tendency to form "smears" or surface coatings during the grinding process can occlude reactive chalcopyrite sites, thereby impeding the accessibility of lixiviants and reducing the overall dissolution flux.

The presence of other sulfide minerals in the concentrate further complicates the leaching environment through electrochemical and chemical interactions:

Table 3. Mineralogical interactions

Mineral	Formula	Rest Potential (V vs. SHE)	Galvanic Role (vs. CuFeS2)	Primary Influence on Dissolution
Pyrite	FeS_2	0.63 - 0.66	Cathodic	Accelerates $CuFeS_2$ oxidation; promotes iron-bearing passivation.
Molybdenite	MoS_2	0.50 - 0.60	Cathodic/Inert	Generally inert; may cause surface masking or subtle galvanic effects.
Sphalerite	ZnS	0.46	Anodic	Preferentially dissolves; can consume lixiviant before $CuFeS_2$ reacts.
Galena	PbS	0.40	Anodic	Rapid dissolution leads to $PbSO_4$ precipitation and surface scaling.

The selective flotation of complex sulfide ores is fundamentally influenced by the electrochemical and chemical interactions that occur between different mineral species in the pulp. These interactions, primarily driven by galvanic coupling and the migration of dissolved ionic species, significantly alter the surface properties of the minerals, often leading to inadvertent activation or depression (Chmielewski & Kaleta, n.d.). When minerals with different rest potentials come into contact, the mineral with the higher potential acts as a cathode, while the one with the lower potential becomes the anode, undergoing accelerated oxidation. This electrochemical synergy not only affects collector adsorption but also facilitates the formation of hydrophilic hydroxide layers or the migration of activating ions, such as, which can severely compromise the selectivity of the separation process (Rao et al., 2024; Zhang & Honaker, 2023). Table 4 summarizes the specific mechanisms and flotation performance impacts resulting from the interaction of common sulfide mineral pairs.

Table 4. Impact of co-existing sulfide minerals on flotation performance

Co-existing Minerals	Mechanism of Interaction	Impact on Flotation Performance	Reference
Chalcopyrite & Pyrite	Galvanic Interaction (Pyrite acts as cathode)	Surface activation of Pyrite by Cu^{2+} ions and surface oxidation of Chalcopyrite, leading to decreased selectivity.	(Chmielewski & Kaleta, n.d.)
Sphalerite & Pyrite	Ion Activation & Surface Coating	Dissolved iron species from Pyrite create a hydrophilic layer on Sphalerite, reducing concentrate grade.	*Rao et al. (2024), Int. Journal of Min. Proc.*

Galena & Pyrite	Galvanic Corrosion	Accelerated surface oxidation of Galena inhibits collector adsorption, resulting in significant recovery loss.	*Zhang & Honaker (2023), Powder Technology*
Arsenopyrite & Pyrite	Surface Chemical Modification	Migration of arsenate ions onto Pyrite surfaces complicates the arsenic-iron separation process.	(*the_kinetics_of_the_dissolution_of_chalc (2)*, n.d.)

2.3. Advanced oxidative leaching strategies to overcome kinetic limitations

To mitigate these limitations and enhance copper extraction efficiency, a wide range of oxidative leaching strategies focusing on either chemical modification or physical activation have been investigated:

Table 5.Oxidative leaching strategies

Category	Description and mechanism	Examples
Chemical Activation	Employing highly aggressive lixiviants or potent redox mediators to bypass the passivating layer or increase the oxidation potential.	Ferric-based Systems (high Fe^{3+}concentration), Chloride-Assisted Leaching (Cl^- acts as a complexing agent to stabilize Cu(I) intermediates and disrupt the passive film), Iodine-Mediated Oxidation, and the use of Strong Chemical Oxidants (e.g., H_2O_2, HNO_3).
Thermo-Hydrometallurgy	Utilizing elevated temperature and pressure to accelerate the reaction rate and chemically decompose the passive layer.	Pressure Oxidation (Autoclave Leaching): High-temperature oxidation of elemental sulfur (S0) to sulfuric acid (H2SO4) effectively removes the primary passivating agent.
Physical Activation	Increasing the available surface area and introducing crystalline defects to provide more reactive sites for lixiviant attack.	Significant size reduction and mechanical activation (strain and defects) enhance the rate of dissolution.

Recent studies underscore the critical importance of understanding the sulfide oxidation mechanism and inter-mineral interactions within these complex concentrates. The application of alternative oxidants and redox mediators has been shown to effectively enhance chalcopyrite dissolution kinetics and attenuate the passivation effects, suggesting promising avenues for developing more efficient and environmentally sound processing technologies.

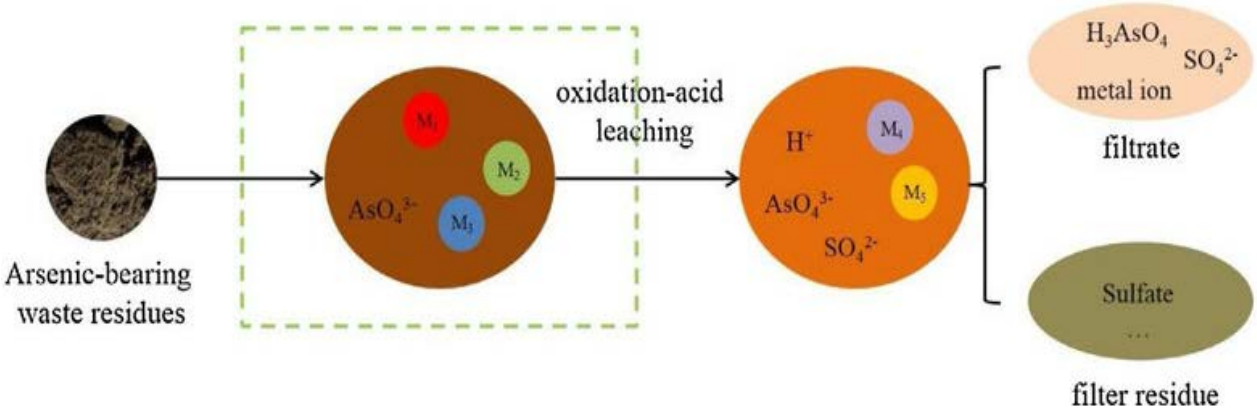


Figure 6. Oxidative leaching process (Yang et al., 2025)

A systematic investigation of copper anode slime has identified a robust two-step oxidation mechanism, demonstrating that the sequential recovery of components can be achieved by precisely tuning the oxidation potential. This aligns with recent advancements in complex sulfide processing, which emphasize the critical importance of understanding inter-mineral interactions and employing alternative oxidants to mitigate passivation effects. Ultimately, these findings underscore that the rigorous control of the electrochemical environment is fundamental to developing efficient and environmentally sound leaching technologies for multi-component mineral systems.

CHAPTER 3: METHODOLOGY

3.1 Introduction

This chapter describes the experimental methodology employed to investigate the leaching behavior of a chalcopyrite ($CuFeS_2$)-dominated copper–molybdenum sulfide concentrates**.** Copper concentrates are generally considered refractory in hydrometallurgical processing due to their slow dissolution kinetics and the formation of surface passivation layers during leaching. Accordingly, the primary objective of this study is to evaluate and quantify the effects of different leaching environments combined with a potent oxidizing agent on copper dissolution efficiency**.** A combined acidic–oxidative hydrometallurgical approach was selected to elucidate the interactions between sulfide minerals and acidic media.

In this study, sulfuric acid (H_2SO_4), hydrochloric acid (HCl), and nitric acid (HNO_3) were employed as leaching media, while ammonium persulfate ($(NH_4)_2S_2O_8$) and iodine (I2) were used as the oxidizing agent. Ammonium persulfate acts as a potent oxidant under acidic conditions, generating reactive oxidizing species that promote the breakdown of sulfide mineral structures. This behavior is particularly effective in overcoming passivation phenomena associated with elemental sulfur formation and the development of iron hydroxide films on mineral surfaces.

During the experimental program, the influencing parameters were systematically varied to evaluate their effects on the leaching performance. These parameters included the type of acidic medium, temperature (20 °C, 50 °C, and 70 °C), the dosage of ammonium persulfate, the dosage of iodine, and the effect of mixed leaching solutions.

For all laboratory-scale experiments, the stirring speed and leaching duration were held constant to ensure comparability across test conditions, while the influence of the selected variables was assessed independently. This chapter investigates the following aspects**:** preparation and homogenization of the copper concentrate, the leaching test protocol, including reagent addition sequence and temperature control, and the analytical techniques applied to both the feed material and leach residues.

These techniques include Atomic Absorption Spectroscopy (AAS) and X-ray Diffraction (XRD), which were employed for quantitative metal analysis and mineralogical evaluation, respectively. In addition, methods for metal recovery calculations and mineralogical interpretation are described.

The selected methodology was designed to generate reproducible and reliable results, enabling a comparative evaluation of different leaching environments in terms of their effectiveness and efficiency. This approach provides a sound basis for interpreting the dissolution behavior of sulfide minerals and for identifying the optimal conditions for copper extraction from sulfide concentrates.

3.2 Experimental Setup and Conditions

3.2.1 Sample Preparation

In this study, a chalcopyrite ($CuFeS_2$) dominated copper concentrate obtained from a copper–molybdenum sulfide deposit was used. The concentrate was produced through a flotation process applied to porphyry-type copper ore. The principal mineralogical composition of the concentrate consisted of chalcopyrite ($CuFeS_2$) as the main copper-bearing phase, accompanied by minor amounts of pyrite (FeS_2) and silicate gangue minerals. The concentrate employed in this investigation is representative of an industrial copper concentrate product recovered from a copper–molybdenum flotation circuit after complete copper–molybdenum separation.

All reagents used in the experimental work were of analytical grade. The leaching media were prepared using sulfuric acid (H_2SO_4), hydrochloric acid (HCl), and nitric acid (HNO_3) at predetermined concentrations. Ammonium persulfate ($(NH_4)_2S_2O_8$), Iodine (I_2) was selected as the primary oxidizing agent due to its high oxidation potential under acidic conditions. In selected experiments, iodine-containing solutions were used to evaluate the effect of mixed oxidizing systems on copper dissolution behavior. Deionized water was used for all solution preparation and dilution to minimize interference from extraneous ions.

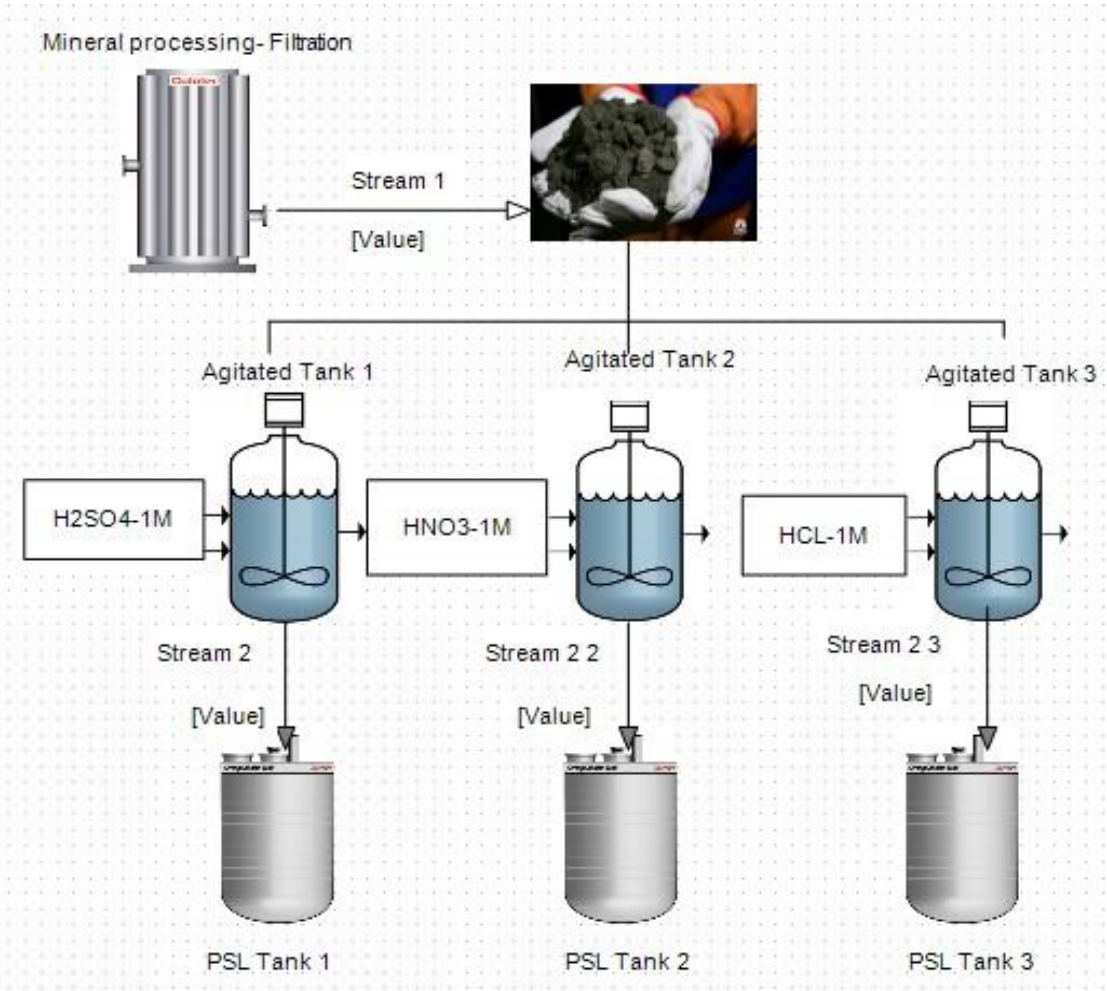


Figure 7.Laboratory test general flowsheet

Prior to leaching experiments, the copper concentrate was subjected to standard sample preparation and homogenization procedures to ensure representativeness and reproducibility of the results. The bulk sample was first oven-dried at 105 °C for 24 hours, then thoroughly mixed to achieve homogeneity. Representative sub-samples were obtained using the coning and quartering method in accordance with standard sampling practices.

The prepared samples were analyzed prior to leaching to determine their elemental composition and mineralogical characteristics. To preserve the original structural and textural features of the concentrate, no additional grinding was applied.

For each leaching test, a known mass of the homogenized concentrate was accurately weighed using an analytical balance and introduced into the leaching reactor containing the pre-prepared leaching solution. Throughout the experimental program, the solid-to-

liquid ratio was maintained constantly to ensure direct comparability between different test conditions.

After leaching, the resulting slurry was filtered to separate the pregnant leach solution (PLS) from the solid residue. The solid residues were thoroughly washed with deionized water, dried, and stored for subsequent mineralogical and surface characterization. The leach solutions were analyzed for copper and iron concentrations, and the results were used to calculate metal extraction and dissolution efficiencies.

3.2.2 Mineralogical characterization of the sample

Research samples underwent mineralogical assessment via XRD and an Automated Mineral Analyzer (TESCAN TIMA), while elemental analysis was conducted through X-ray Fluorescence (XRF) spectroscopy.

The phase distribution and mineralogical compositions of the sample are depicted in the following images.

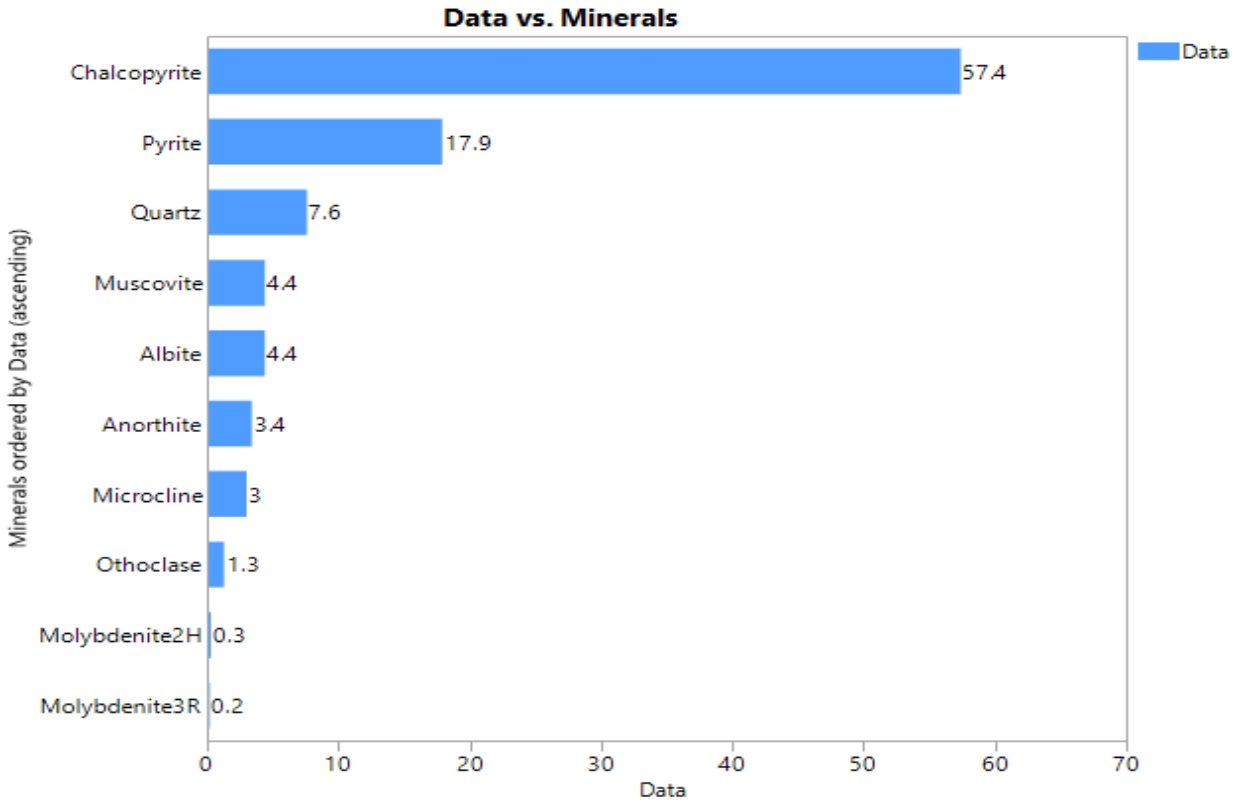


Figure 9. Sample XRD analysis report

The sample is predominantly composed of sulfide minerals (75.8%) and silicate-based gangue minerals (24.2%). The primary value-bearing mineral is Chalcopyrite, with Molybdenite present as a significant by-product.

Table 6 . Copper concentrates mineral XRD report

Mineral Category	Mineral Name	Formula	Weight (%)
Primary Sulfide	Chalcopyrite	$CuFeS_2$	57.4
Secondary Sulfide	Pyrite	FeS_2	17.9
By-product	Molybdenite (2H+3R)	MoS_2	0.5
Silicates (Feldspars)	Albite, Anorthite, Microcline, Orthoclase	$(Na,Ca,K)AlSi_3O_8$	12.1
Silicates (Phyllosilicates)	Muscovite	$KAl_2(AlSi_3O\{10\})(OH,F_2)$	4.4
Oxides	Quartz	SiO_2	7.6

Chalcopyrite at 57.4% the theoretical copper grade of this concentrate is approximately 19.8-20.1% Cu. This is a standard commercial-grade concentrate, though it suggests some dilution. Pyrite's concentration of 17.9% indicates significant iron sulfide enrichment. High pyrite content increases the sulfur-to-copper ratio, requiring greater oxygen enrichment during the smelting process. Molybdenite is a key mineralogical indicator of the presence of both 2H and 3R polytypes. The 2H polytype is typical for most porphyry systems, while 3R can sometimes indicate specific geochemical conditions or higher rhenium concentrations.

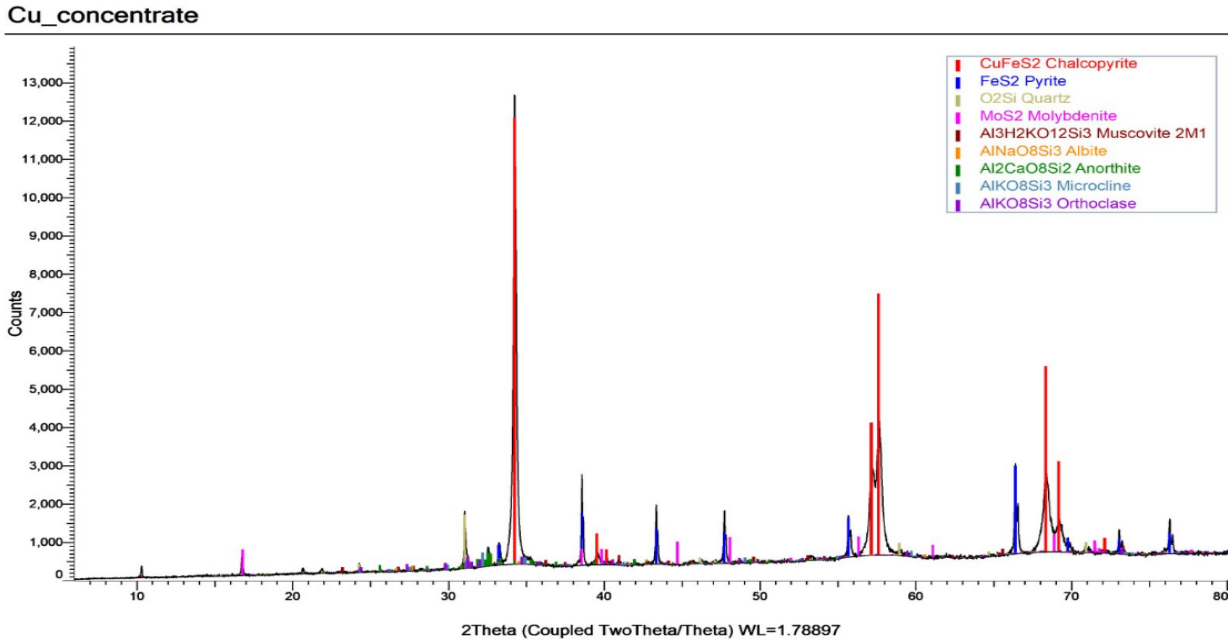


Figure 8. XRD peak profile of the original concentrate (experimental feed)

The non-sulfide gangue totals 24.2%, which impacts the due to penalties or increased processing costs. The combination of quartz (7.6%) and feldspars (12.1%) contributes to the total SiO_2 and Al_2O_3 load.

The 4.4% Muscovite content is critical for flotation kinetics. micaceous minerals tend to report to the concentrate through entrainment or "sliming," which can hinder the selectivity of chalcopyrite recovery. The comprehensive mineralogical characterization of the feed material, conducted prior to the leaching experiments as per the sampling procedures described above, revealed. The concentrate is primarily composed of 57.4% chalcopyrite and 17.9% pyrite. This initial mineralogical state serves as the benchmark for evaluating the subsequent efficiencies of copper and iron extraction and dissolution.

A detailed characterization of the mineralogical composition, intergrowth, and liberation degrees within the study samples was performed using an automated mineralogy system. This analysis enabled the determination of optimal processing parameters, which are detailed in the following section.

Automated mineralogy system based on Scanning Electron Microscopy (SEM). This instrument provides rapid, automated, detailed mineralogical analysis to determine key parameters that influence the beneficiation process. These parameters include:

- Mineralogical composition
- Textural characteristics (Grain size and particle size distribution)
- Mineral association (Intergrowth)
- Degree of liberation

Furthermore, the system features a specialized measurement mode called Bright Phase Search (BPS), designed to automate the detection and characterization of heavy elements, such as gold and platinum-group minerals (PGM).

Table 7. Size fractionated elemental analysis

Elements / Fraction	Cu concentrate +20	Cu concentrate -20
Hydrogen	0.0367	0.0125
Carbon	0.0313	0.009
Oxygen	12.7789	1.8393
Fluorine	0.0568	0.0092
Sodium	0.3262	0.0396
Magnesium	0.0752	0.0159
Aluminum	2.1024	0.3987
Silicon	8.6731	1.0844
Phosphorus	0.0277	0.0059
Sulphur	29.6661	36.3059
Potassium	0.917	0.1513
Calcium	0.1549	0.043
Titanium	0.1874	0.0499
Iron	25.2296	30.7045
Copper	18.6319	28.0534
Zinc	0.6355	0.7943
Arsenic	0.0775	0.1542
Strontium	0.013	0.0061
Yttrium	0.001	0
Zirconium	0.004	0
Molybdenum	0.3028	0.2631
Antimony	0.0043	0.0096
Barium	0.0084	0.0079
Lanthanum	0.0011	0.0007
Cerium	0.0083	0.0017
Neodymium	0.0009	0.0006
Lead	0.0471	0.0384
Thorium	0.0004	0.0002
Rare earth elements	0.0007	0.0005
Total	**100**	**100**

The sharp increase in copper grade to 28.05% alongside the reduction of silicon to its minimum level of 1.08% within the -20μm fraction demonstrates that fine-grained chalcopyrite has achieved near-complete liberation from the gangue matrix, reporting as a distinct pure phase. This observation serves as a critical parameter for establishing the optimal degree of comminution.

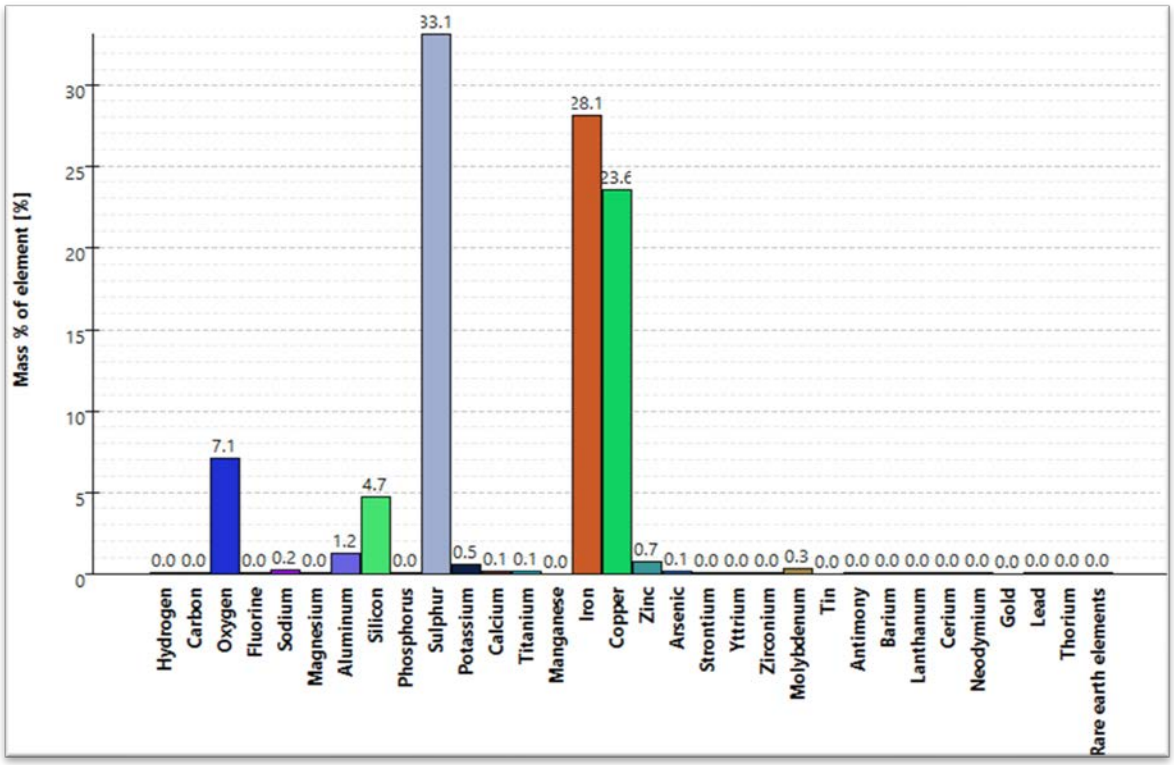


Table 8. Elemental mass of the sample

The elemental distribution across size fractions suggests that a differential leaching strategy could be beneficial. The -20μm fraction, with its superior copper grade (28.05%) and minimal silicate interference (1.08% Si), is highly suitable for rapid chemical leaching. Conversely, the coarse +2μm fraction may require intensive pre-treatment or mechanical activation to overcome the physical barrier posed by the 8.67% Si and 12.77% O-bearing gangue matrix before hydrometallurgical processing.

- **Liberation kinetics and category classification result of the advanced automated mineralogy solution:**

The "Category Viewer" results (Fig. 8) demonstrate that chalcopyrite liberation is size-dependent. Particles were categorized based on their chalcopyrite mass percentage:

- Liberated Particles (80%): A high proportion of fully liberated chalcopyrite is evident in both fractions, indicating effective primary comminution.
- Middlings (20-80): These particles consist of chalcopyrite complexly intergrown with pyrite and silicates. These binary and ternary associations are critical as they often report to the scavenger circuits or dilute the final concentrate grade.

- Locked Particles (<20): Fine chalcopyrite inclusions within gangue matrices identify the limit of physical separation under current grinding conditions.

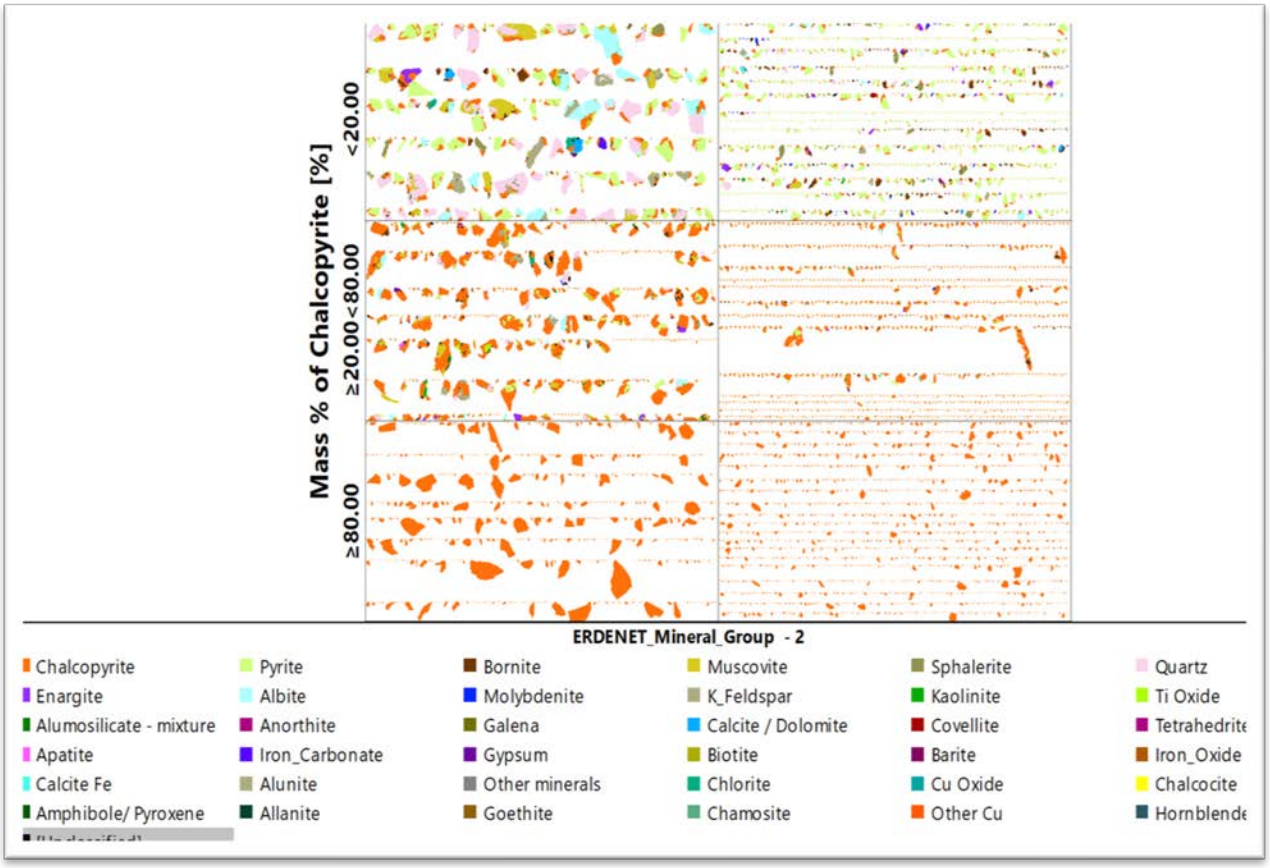


Figure 10. Category of fraction concentrate

The analytical results indicate that while chalcopyrite liberation within the copper concentrate is relatively high, significant intergrowth with pyrite and silicates remains prominent in the +20 µm size fraction. Figure 9 illustrates the panoramic images of the measured sample.

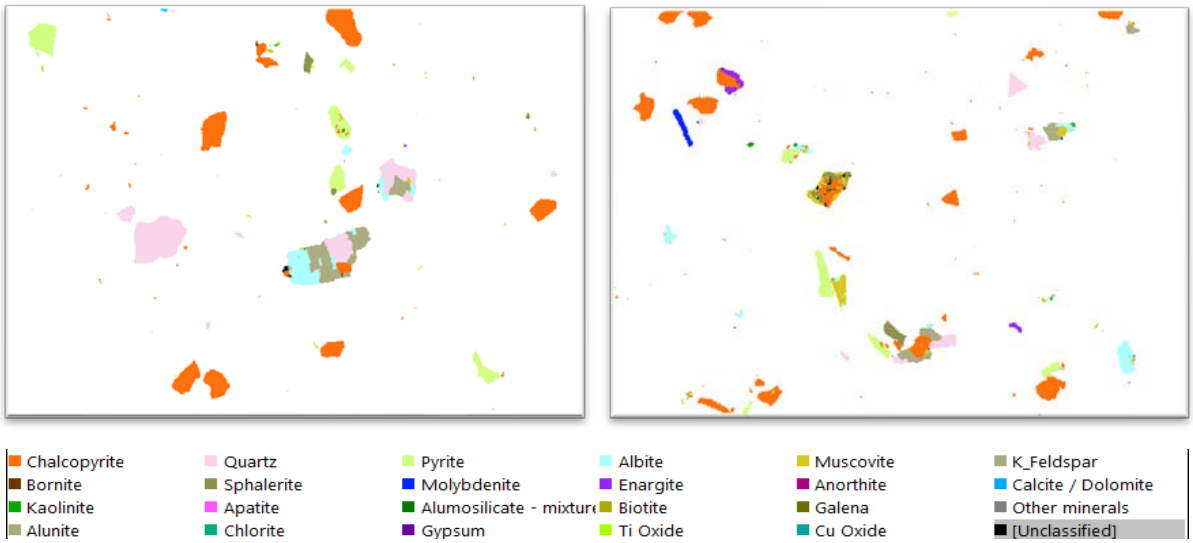


Figure 11. Panoramic result of the sample

The identification of complex intergrowths between chalcopyrite and silicate gangue minerals suggests that ultra-fine grinding may be required to increase the effective surface area for leaching. Furthermore, the dominance of chalcopyrite ($CuFeS_2$) underscores the need to manage the passivation layer to ensure efficient copper extraction in acidic media.

Table 9. Comparative Mineralogical Composition by Size Fraction

Parameter	+20 µm Fraction (Coarse)	-20 µm Fraction (Fine)	Metallurgical Significance
Primary Mineral	Chalcopyrite ($CuFeS_2$) ~55%	Chalcopyrite ($CuFeS_2$) ~78%	Significant enrichment of copper sulfide in the finer fraction due to improved mineral liberation.
Associated Sulfide	High Pyrite (FeS_2) content (~20%)	Low Pyrite (FeS_2) content (<5%)	Demonstrates high selectivity of the flotation process in finer size ranges, effectively depressing pyrite.
Gangue Minerals	Significant Silicates (Quartz, Albite, Muscovite)	Trace amounts of Silicates and Aluminosilicates	Indicates that coarse fractions contain more "locked" particles (interlocked with waste rock).
Liberation Status	Partially Liberated / Interlocked	Highly Liberated	The -20 µm fraction represents a high-grade concentrate, while +20 µm may require re-grinding.
Concentrate Grade	Estimated 18-20% Cu	Estimated 26-28% Cu	Shows a direct correlation between particle size reduction and final copper grade.

The mineralogical characterization of the Erdenet copper concentrate reveals a distinct partitioning of phases between the size fractions. The +20 µm fraction is characterized by a high proportion of gangue minerals and pyrite, suggesting insufficient liberation of chalcopyrite at coarser sizes. Conversely, the -20 µm fraction shows a significant

upgrade in chalcopyrite content (~78%), indicating that the fine grinding effectively liberates the target copper minerals from the silicate matrix. These results suggest that optimizing the re-grinding circuit could further enhance the overall copper recovery and concentrate grade by targeting the locked particles in the coarser fractions.

- **Mass of copper in phase**

These data represent a critical analysis of copper elemental deportment, detailing the distribution of copper across various mineral phases within the concentrate and their respective percentages. The analytical results for the research sample are presented in the figure below.

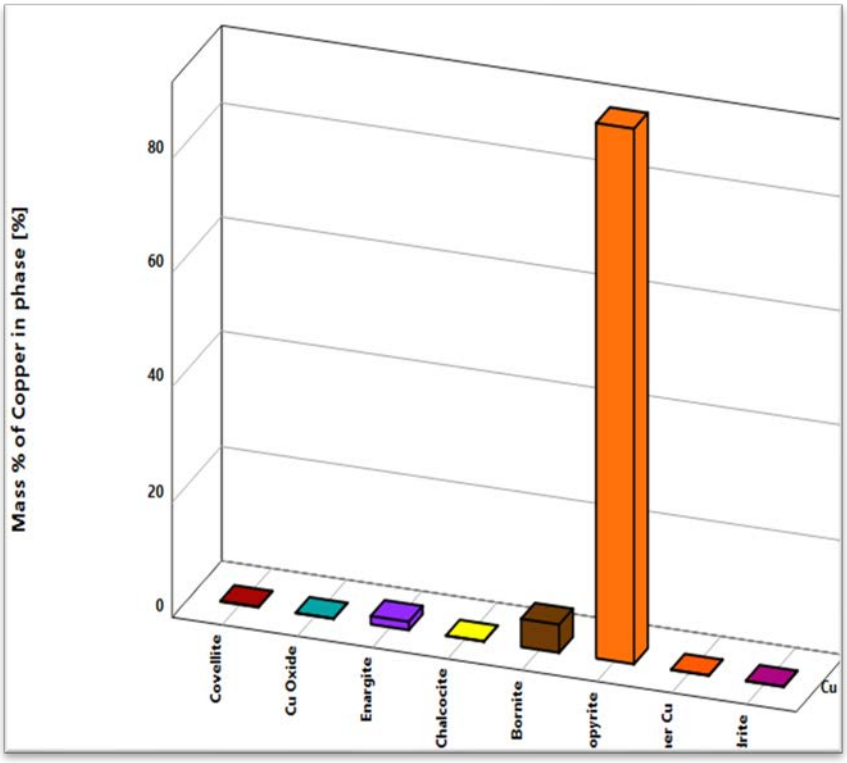


Figure 12.Copper Elemental Deportment by Mineral Phase

The mineralogical assessment demonstrates that while the concentrate is dominated by refractory chalcopyrite (93.48%), the high enrichment in the -20 µm fraction provides a strategic advantage for atmospheric stirred tank leaching. The presence of Enargite further justifies a hydrometallurgical approach over pyrometallurgy to effectively

sequester arsenic as a stable solid waste. Therefore, the processing route should focus on catalytic leaching to overcome the passivation of primary sulfides.

3.2.2 Experiment DOE

Framework of the Experimental Design

To investigate the leaching behavior of chalcopyrite ($CuFeS_2$), a systematic multi-variable experimental matrix was established. The primary objective was to evaluate how various lixiviants and thermal regimes influence the breakdown of the mineral matrix. The study focused on three critical factors: the nature of the acidic medium, the concentration of oxidizing agents, and the impact of catalytic additives.

3.2. Variables and Operational Parameters

The research was conducted under controlled batch conditions, where the following independent variables were manipulated:

- Thermal Gradient: Tests were performed at 20°C, 50°C, and 70°C to ascertain the energy activation requirements.
- Lixiviant Systems: Comparative trials were executed using H_2SO_4, HCl, and HNO_3 as base acids.
- Chemical Additives: Ammonium persulfate $(NH_4)_2S_2O_8$ served as the high-potential oxidant, while molecular iodine (I2) was utilized to evaluate its catalytic efficacy in bypassing mineral passivation.

Experiments were carried out in a temperature-controlled glass reactor with continuous mechanical agitation to ensure uniform mass transfer. Aliquots of the Pregnant Solution Liquid were extracted at predefined intervals (2, 4, 6, and 24 hours). These samples were subsequently filtered and subjected to elemental analysis to determine the recovery rates of copper and iron.

As depicted in Figure 8, the quantitative analysis of copper dissolution in the PSL revealed a significant variation with lixiviant composition. The data underscores a robust positive correlation between thermal input and leaching efficiency.

The most striking result was observed at 70°C, where the HCl+ Ammonium Persulfate + Iodine system yielded a peak copper mass of 164 mg. This suggests that at elevated temperatures, the chloride environment facilitates superior ion transport compared to sulfate or nitrate media. Conversely, under ambient conditions (20°C), the HNO_3 based

system exhibited the highest initial reactivity (57.6 mg), likely due to the nitrate ion's inherent oxidative properties. However, the plateauing of HNO_3 performance at higher temperatures suggests that the chloride-persulfate-iodine synergy is more effective for deep mineral degradation.

Kinetic Profiles and Passivation Behavior

A critical observation is the synchronization between copper recovery and iron dissolution. At 70°C, copper recovery approached 90% within the 24-hour sampling window. The sharp upward trajectory of the recovery curve between 6 and 24 hours indicates the successful mitigation of the passivation layer. In contrast, at 20°C, the recovery rate remained stagnant, failing to exceed the 20% threshold.

It confirms that the dissolution of chalcopyrite is a chemically controlled process in which the energy barrier to breaking the metal-sulfur bonds is significant, requiring either high thermal energy or potent catalytic mediation.

The experiment find corroborate that the oxidative leaching of chalcopyrite is highly sensitive to both the chemical environment and the thermal regime. The integration of Hydrochloric acid, Ammonium Persulfate, and Iodine at 70°C emerged as the optimal configuration for maximizing copper extraction. The kinetic studies demonstrated that a 24 hours residence time is sufficient for near-complete dissolution under high-temperature conditions. Furthermore, the use of iodine as a catalyst presents a viable technological pathway to enhance recovery rates at lower temperatures, potentially reducing the overall energy consumption of the hydrometallurgical process. This study successfully identifies a synergistic reagent balance that overcomes mineral passivation, providing a robust framework for future industrial scale-up.

The experimental design was developed using JMP Pro statistical software to systematically evaluate the effects of key process variables, including acid type, temperature, and oxidizing agent conditions. The Design of Experiments (DOE) module in JMP Pro was employed to generate an efficient experimental matrix that minimized the number of tests while preserving statistical significance. This structured approach enabled reliable assessment of both main effects and interaction effects on leaching performance. Figure 8 shows the experiment DOE by JMP Pro statistical program.

3.2.3 Leaching experimental process

The leaching experiments were conducted using a laboratory-scale, well-controlled experimental setup designed to simulate hydrometallurgical processing conditions while enabling precise control and monitoring of the factors influencing mineral dissolution. The following equipment and operating conditions were employed:

Custom Design

Responses

Factors

Define Factor Constraints

- None
- Specify Linear Constraints
- Use Disallowed Combinations Filter
- Use Disallowed Combinations Script

Model

Alias Terms

Design

Run	Oxidizing agent	Temperature	Enhancing oxidant	Leaching time, hour	Volume, ml	Copper concentrate mass,gr
1	H2SO4-1M	20	Ammonium persulfate	24	100	1
2	H2SO4-1M	20	Iodine	24	100	1
3	H2SO4-1M	50	Ammonium persulfate	24	100	1
4	H2SO4-1M	50	Iodine	24	100	1
5	H2SO4-1M	70	Ammonium persulfate	24	100	1
6	H2SO4-1M	70	Iodine	24	100	1
7	HCl-1M	20	Ammonium persulfate	24	100	1
8	HCl-1M	20	Iodine	24	100	1
9	HCl-1M	50	Ammonium persulfate	24	100	1
10	HCl-1M	50	Iodine	24	100	1
11	HCl-1M	70	Ammonium persulfate	24	100	1
12	HCl-1M	70	Iodine	24	100	1
13	HNO3-1M	20	Ammonium persulfate	24	100	1
14	HNO3-1M	20	Iodine	24	100	1
15	HNO3-1M	50	Ammonium persulfate	24	100	1
16	HNO3-1M	50	Iodine	24	100	1
17	HNO3-1M	70	Ammonium persulfate	24	100	1
18	HNO3-1M	70	Iodine	24	100	1

Figure 8. Experiment DOE

a) Oxidized leaching:

Laboratory leaching tests were carried out in 250 mL borosilicate glass reactors, placed in a temperature-controlled water bath to maintain a stable, uniform temperature throughout the reaction period.

b) Continuous agitation:

To maintain a homogeneous reaction environment and to enhance interactions between the solid and liquid phases, continuous agitation was applied using a magnetic stirrer. The stirring speed was fixed at 400 rpm, which was sufficient to prevent particle settling and to ensure effective mass transfer.

c) Leaching temperature:

The reaction temperature was maintained at 20 °C, 50 °C, or 70 °C, depending on the experimental conditions. These three temperature levels were selected to

evaluate the influence of temperature on leaching kinetics and passivation behavior.

d) pH and ORP monitoring:

During the leaching process, changes in solution chemistry were continuously monitored in real time using calibrated pH electrodes and oxidation–reduction potential (ORP) electrodes. pH measurements provided information on the solution's acidity or alkalinity, allowing assessment of lixiviant activity and hydrolysis reactions occurring during leaching. ORP measurements were vital for evaluating the effectiveness and consumption of the oxidizing agent and for verifying whether the oxidation potential required to accelerate or activate the leaching reactions was consistently maintained.

e) Sampling and filtration:

Solution sampling was performed at 2-hour intervals during leaching. After 24 hours of leaching, the slurry was filtered to separate the solid and liquid phases. The solid residues were thoroughly washed with deionized water, dried, and preserved for subsequent mineralogical and surface analyses, including X-ray diffraction (XRD).

f) Solid-to-liquid ratio:

The leaching experiments were conducted using a solid mass of 1 g and a solution volume of 100ml. This concentration was selected as it provides an appropriate balance between studying leaching kinetics and ensuring sufficient analytical accuracy.

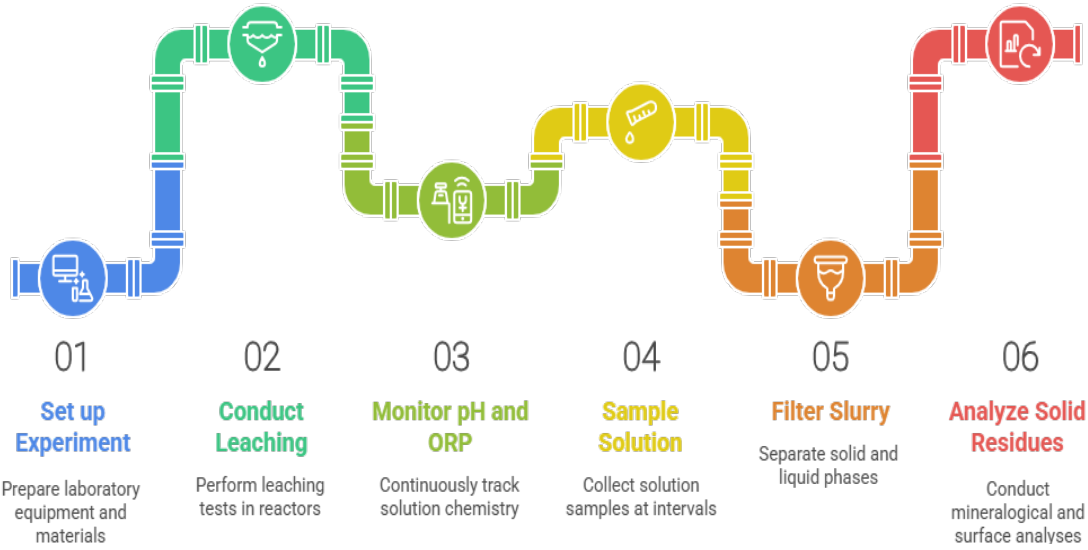


Figure 9. Leaching experiment process

This carefully controlled laboratory environment ensured the accuracy and reliability of the experimental results. By maintaining constant and standardized conditions—such as temperature, stirring speed, and reagent dosages- the reproducibility of the leaching experiments was ensured. Moreover, the fully controlled setup enabled a direct comparison of leaching performance, allowing the effects of individual experimental parameters on leaching efficiency to be evaluated clearly and objectively.

3.2.4 Leaching Agents and Reagents

In this study, I investigated how the combined effect of different acidic media and potent oxidizing agents, including an iodine-based system, influences the leaching behavior of a chalcopyrite-dominated copper concentrate. The primary objective of the work was to identify leaching conditions capable of enhancing copper dissolution from chalcopyrite, which is well known for its slow leaching kinetics and strong tendency toward surface passivation under conventional hydrometallurgical conditions.

Based on leaching performance, industrial relevance, and chemical reactivity, I selected three mineral acids to establish the leaching environment:

1. **Nitric acid (HNO_3)**

Nitric acid was chosen due to its intrinsic oxidizing character, which enables direct attack on the sulfide matrix and promotes the dissolution of both copper and iron species.

Nitric acid was included in the study because of its dual role as a proton donor and a potent oxidizing agent. Unlike non-oxidizing acids, HNO_3 initiates a direct oxidative attack on the stable sulfide matrix. Theoretically, the nitrate ion (NO_3) facilitates the rapid oxidation of sulfide sulfur (S_2) not only to elemental sulfur (S^0) but also to higher oxidation states, such as sulfate (SO_4^{2-}). This deep oxidation is crucial because it disrupts the formation of the dense, sulfur-rich film that typically halts dissolution in other media. In a mixed system with Ammonium Persulfate, HNO_3 is expected to exert an autocatalytic effect, in which nitrogen oxide intermediates further accelerate electron transfer from the mineral surface to the bulk solution.

2. Hydrochloric acid (HCl)

Hydrochloric acid was employed to assess the role of chloride complexation in accelerating copper dissolution and mitigating passivation effects. Hydrochloric acid was selected to investigate the "chloride effect," which is widely recognized for enhancing the leaching kinetics of refractory copper concentrates. The theoretical advantage of HCl lies in the aggressive nature of chloride ions (Cl) as ligands. Chloride ions promote the formation of stable aqueous complexes, such as tetrachlorocuprate ($[CuCl_4]^{2-}$), which lowers the activity of free Cu^{2+} at the mineral interface and drives the dissolution reaction forward.

3. Sulfuric acid (H_2SO_4)

Sulfuric acid, the most widely used acid in industrial hydrometallurgy, was adopted as a reference medium to evaluate the dissolution behavior of copper and iron under sulfate-dominated conditions. Sulfuric acid remains the cornerstone of industrial hydrometallurgy due to its cost-efficiency and compatibility with downstream Solvent Extraction and Electrowinning (SX-EW) processes. In this research, H_2SO_4 serves as the baseline reference. Theoretically, chalcopyrite leaching in pure sulfate media is plagued by slow kinetics and the precipitation of secondary phases like jarosite which further contribute to surface passivation.

To allow direct comparison between systems, all acids were used at a fixed concentration of 1.0 M.

As the principal oxidizing agent, I used ammonium persulfate ($(NH_4)_2S_2O_8$) in all leaching systems. Under acidic conditions, this reagent generates highly reactive species such as sulfate radicals ($SO_4^{\bullet -}$) and peroxydisulfate ions ($S_2O_8^{2-}$), which can

disrupt the crystal lattice of refractory sulfide minerals. I selected ammonium persulfate because of its strong oxidation potential and its reported ability to overcome passivation phenomena commonly associated with chalcopyrite dissolution.

In addition, selected experiments were conducted using an iodine/iodide (I_2/I^-) redox system as a supplementary oxidizing component. I considered this system particularly relevant because it can participate in reversible redox cycling, thereby sustaining oxidative conditions at the mineral surface. The iodine-based system was introduced to facilitate the removal or modification of elemental sulfur layers and to enhance electrochemical reaction rates at the chalcopyrite surface.

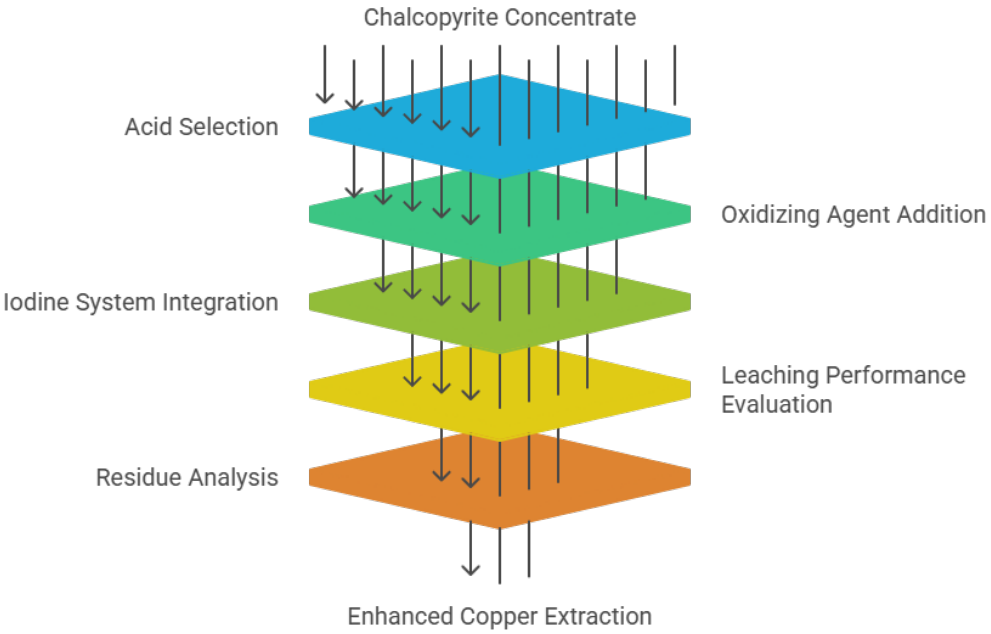


Figure 10. Chalcopyrite leaching process

A combined acidic–persulfate–iodine leaching environment would reduce the formation of passivating surface products, such as elemental sulfur and iron hydroxide or jarosite-type precipitates, thereby improving copper extraction efficiency. Leaching performance was evaluated by monitoring copper extraction over time, while post-leach solid residues were examined using X-ray diffraction (XRD) and scanning electron microscopy (SEM) to elucidate mineralogical transformations and surface alterations induced during leaching.

3.2.5 Experimental Procedures

This section describes the step-by-step procedure for conducting combined acid and oxidant leaching tests on the copper sulfide concentrate. The procedure includes sample preparation, leaching execution, and post-leaching analysis to evaluate metal dissolution and mineralogical changes.

1. Sample and Leaching Solution Preparation

Sample Preparation: A copper concentrate sample was collected from the loading section of the Erdenet Mining Corporation. The sample was transported to the laboratory and dried at 105°C for 24 hours. Following the drying process, the sample was homogenized, and a representative portion was sub-sampled after spreading. After thorough re-mixing of the representative sample, a 1.0 g aliquot for the leaching process was prepared using an analytical balance."

A representative sample of 1 gram of previously homogenized and dried copper sulfide concentrate was accurately weighed using an analytical balance.

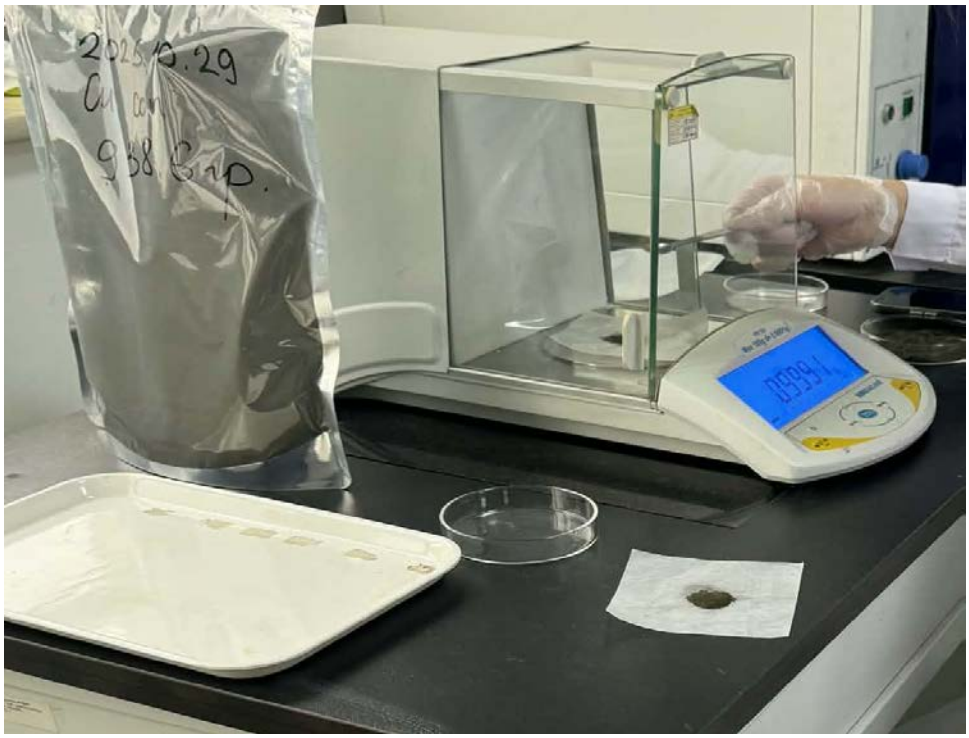


Figure 11. Sample preparation for laboratory experiment

- Acid Solution Preparation

A volume of 100 ML of the selected sulfuric acid (H_2SO_4), nitric acid (HNO_3), or hydrochloric acid (HCl) was prepared at the desired molar concentration 1M using analytical grade reagents and deionized water.



Figure 12. Acid solid preparation process

- Oxidant Preparation:

An initial dosage of 1 gram of ammonium persulfate ($(NH_4)_2S_2O_8$) was measured and reserved as the oxidizing agent. This dosage was selected based on preliminary tests and was further optimized in subsequent experiments.



Figure 13. Sample and leach solution preparation

Leaching setup

- The prepared acid solution was transferred to a 250 mL borosilicate glass beaker positioned on a stirred hot plate with temperature control.
- The copper concentrate sample was gradually introduced into the acid solution while stirring to ensure uniform dispersion.
- The pre-measured ammonium persulfate was immediately added to the reactor before the onset of heating to initiate the oxidizing environment.
- The reactor temperature was adjusted to the target condition (20°C, 50°C, or 70°C) using the integrated temperature control system on the hot plate.

  A magnetic stir bar was used to maintain continuous agitation throughout the experiment, ensuring homogeneous mixing and adequate contact between the solid and the leaching solution.



Figure 14. Leaching process – at ambient temperature (20ºC) and 400 rpm

Leaching Conditions

- The leaching reaction was allowed to proceed for 24 hours under constant agitation (typically 400 rpm).
- Throughout the test, pH and temperature were periodically monitored using calibrated pH and ORP (oxidation-reduction potential) probes to track the evolution of solution chemistry.
- No external pH adjustment was made during the experiment to simulate batch leaching behavior, except in specific optimization tests.

2. Filtration and Sampling

- Leachate samples were extracted at predetermined time intervals—2, 4, 6, and 24 hours—using a syringe and immediately filtered through 0.45 µm syringe filters to remove suspended solids.
- After 24 hours, the entire slurry was subjected to vacuum filtration using a Büchner funnel to separate the leachate from the solid residue.
- The solid residue was thoroughly washed with deionized water to remove any adhering leach solution, then dried at 60°C in an oven for subsequent mineralogical characterization.

- The liquid phase (filtrate) was preserved in sealed containers and acidified (if necessary) for elemental analysis.



FIGURE 15. FILTRATION AND SAMPLING PROCESS

The recovered leachate was analyzed for copper (Cu) and iron (Fe) using Inductively Coupled Plasma Mass Spectrometry (ICP-MS) or Atomic Absorption Spectroscopy (AAS), depending on availability and required detection limits.

Safety Measures

Risks associated with the use of sulfuric acid (H_2SO_4) during electrolysis were minimized by wearing comprehensive personal protective equipment (PPE) throughout the experiment. This included acid-resistant gloves, safety goggles, and laboratory coats.

To ensure the safe discharge of any gas vapors or acid mists generated during the procedure, a continuous ventilation system was maintained, and all experimental activities were conducted within a specialized fume hood.

3.3 Analytical Techniques and Data Collection

To evaluate the effectiveness of leaching and the extent of metal recovery, a comprehensive suite of analytical techniques was employed. These methods were selected to quantify dissolved metal concentrations, assess changes in mineralogy, and monitor the leaching environment throughout the experiments.

- Atomic Absorption Spectroscopy (AAS):

A complementary technique used to verify copper in solution. AAS is beneficial for confirming ICP-MS results and is less sensitive to matrix interferences, which can be helpful in leachate analysis.

- X-ray Powder Diffraction (XRPD):

XRPD was employed to identify the crystalline phases present in the solid residues before and after leaching. This technique provides information on mineralogical transformations and can detect the formation or dissolution of specific sulfide and oxide phases. XRPD data were analyzed using ICSD reference patterns to match known mineral structures, such as chalcopyrite, bornite, pyrite, and molybdenite.

3.4 Data Analysis and Calculations

The data collected from the leaching experiments were carefully analyzed to quantify leaching efficiency, model reaction kinetics, and evaluate reproducibility.

Leaching Efficiency

Leaching efficiency was calculated using the following formula:

$$\text{Recovery (\%)} = Ct * V / mi * 100 \qquad (1)$$

Where:

C_t: Concentration of the metal in solution at time t (measured by AAS)

V: Volume of the leach solution.

m_i: Initial mass of the metal in the sample

This equation allows for the quantification of copper and other metal recoveries at various stages of the leaching process, providing insights into the effectiveness of the leaching agents and conditions.

Kinetic Modeling

To understand the dissolution rates of chalcopyrite and bornite, the experimental data were fitted to kinetic models:

- Shrinking Core Model: This model is commonly used to describe the leaching of solid sulfide minerals, where the reaction proceeds at the surface of the particle and then progresses inward as the core shrinks.
- Diffusion-Controlled Process: In some cases, the leaching rate is controlled by the diffusion of leachant to the surface of the particles, particularly if a passivating layer forms.
- By analyzing the kinetic data, the reaction rate constants and mechanisms controlling the leaching process were identified.

Experimental results indicate that the leaching of chalcopyrite is limited by diffusion through the product layer (sulfur layer) formed on the solid surface. This was calculated using the following Shrinking Core Model (SCM) equation for product layer diffusion:
The apparent rate constants (k) were determined using the Shrinking Core Model (SCM) for product-layer diffusion at various temperature intervals (hours).

Table 10. Calculated kinetic rate constants

Temperature (K)	Temperature (°C)	Recovery (X)	Rate Constant (k, hr−1)
293 K	20°C	0.102	1.54×10^{-4}
323 K	50°C	0.521	4.29×10^{-3}
343 K	70°C	0.899	2.30×10^{-2}

Activation Energy (E_a) and Arrhenius Plot

The relationship between the reaction rate constant and temperature was expressed using the Arrhenius equation to determine the activation energy:

$$lnk = lnA - \frac{E_a}{RT}$$

Where:

- k: The reaction rate constant (calculated from the Shrinking Core Model).
- A: The pre-exponential factor (frequency factor).
- E_a: The activation energy of the reaction (J/mol or kJ/mol).
- R: The universal gas constant (8.314J/mol*K).
- T: The absolute temperature in Kelvin (K).

By plotting against the reciprocal of the temperature (1/T), a straight line is obtained. The slope of this line represents -E_a/R.

Based on the experimental data:

- Slope of the plot: ≈ -10.265
- Calculated: E_a: $\approx 85.3 kJ/mol$

  The apparent activation energy (85.3 kJ/mol) is well above the commonly used ~40 kJ/mol criterion, strongly indicating that chalcopyrite leaching in the HNO_3 + $(NH_4)_2S_2O_8$ system is predominantly controlled by surface chemical reactions rather than mass-transfer (diffusion) through the boundary/product layer. Therefore, the rate-limiting step is most likely associated with the surface oxidation/dissolution reaction of chalcopyrite.

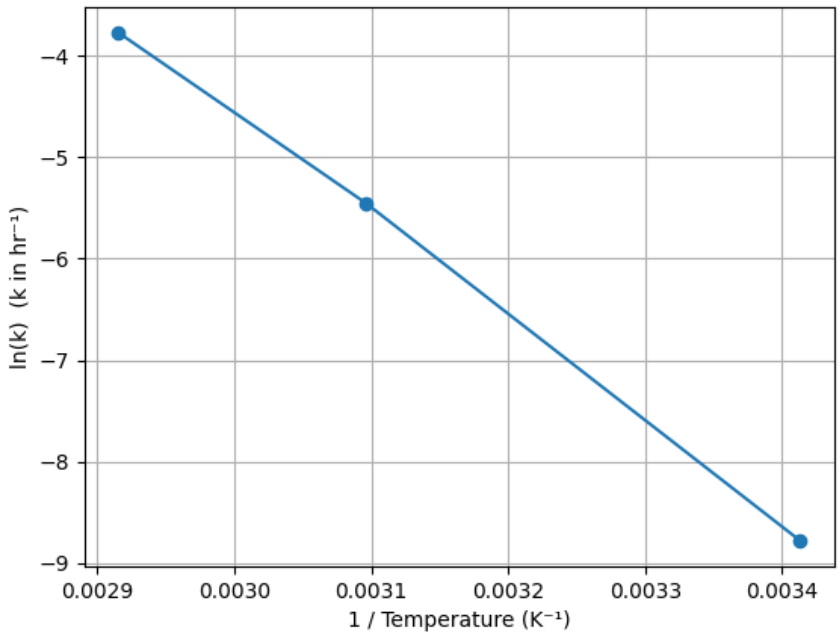


Figure 14. Arrhenius plot

Figure shows the Arrhenius plot of ln k versus 1/T for chalcopyrite leaching. The linear relationship indicates that the reaction follows Arrhenius behavior. The apparent activation energy (≈84–85 kJ mol^{-1}), obtained from the slope of the plot, is significantly higher than values typically associated with diffusion-controlled processes, confirming that chalcopyrite leaching in this system is predominantly controlled by surface chemical reactions rather than mass-transfer limitations.

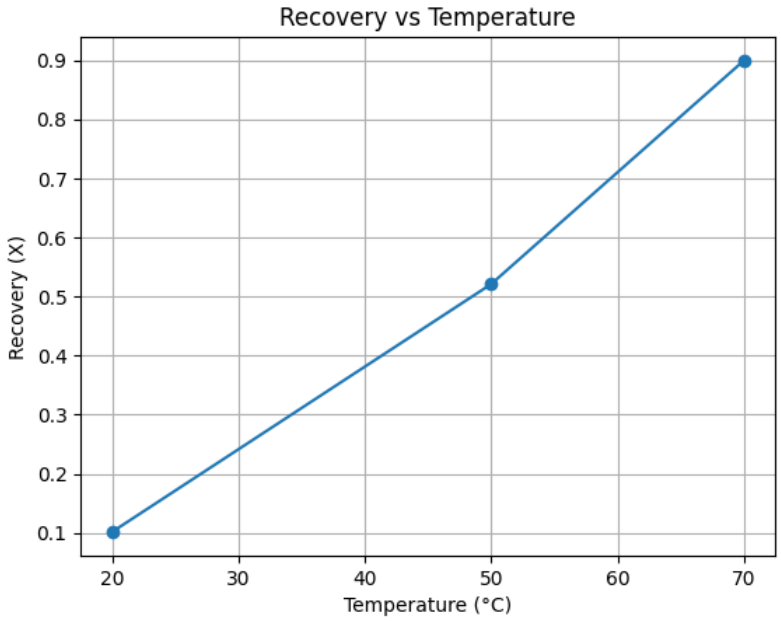


Figure 15. Effect of temperature on chalcopyrite leaching recovery

The figure illustrates the effect of temperature on chalcopyrite leaching recovery. The copper recovery increases sharply with temperature, rising from approximately 10% at 20 °C to nearly 90% at 70 °C. This strong temperature dependence indicates that the leaching process is kinetically controlled by surface chemical reactions rather than diffusion. The observed trend is consistent with the high apparent activation energy obtained from the Arrhenius analysis.

Statistical Analysis

To ensure the reliability of the results, statistical methods were employed:

- Standard Deviation: The variability of the experimental data was quantified using the standard deviation, ensuring that the results were statistically significant and reproducible.

- Error Analysis: Measurement errors were calculated for each analytical technique, and corrections were made to ensure the accuracy of the results.

Limitations of the Methodology

While the methodology employed provides valuable insights into the leaching behavior of chalcopyrite and bornite, several limitations must be acknowledged:

Laboratory-Scale Limitations

The experiments were conducted under controlled laboratory conditions, which may not fully represent the complexities of large-scale industrial processes. Factors such as temperature fluctuations, leachant composition, and particle size distribution may differ in a real-world mining operation.

Impurities in the Ore

The study focused on copper sulfide concentrates, but impurities (such as arsenic, antimony, or other trace elements) in the ore matrix may influence metal recovery. Impurities could affect the efficiency of leaching agents and complicate the overall process.

Reaction Kinetics Variability

Reaction kinetics can vary depending on factors such as particle size and the chemical composition of the leach solution. Variations in these factors may lead to differences in dissolution rates and passivation layer formation, which were nOT fully accounted for in this study.

CHAPTER 4: RESULTS AND DISCUSSION

4.1 Effect of Oxidants

In the leaching process of chalcopyrite ($CuFeS_2$), the primary role of the oxidant is to decompose the passivation layer formed on the mineral surface and to facilitate the conversion of sulfide sulfur ($S2^{-)}$ into elemental sulfur (S0) or sulfate ($SO42^{-}$).

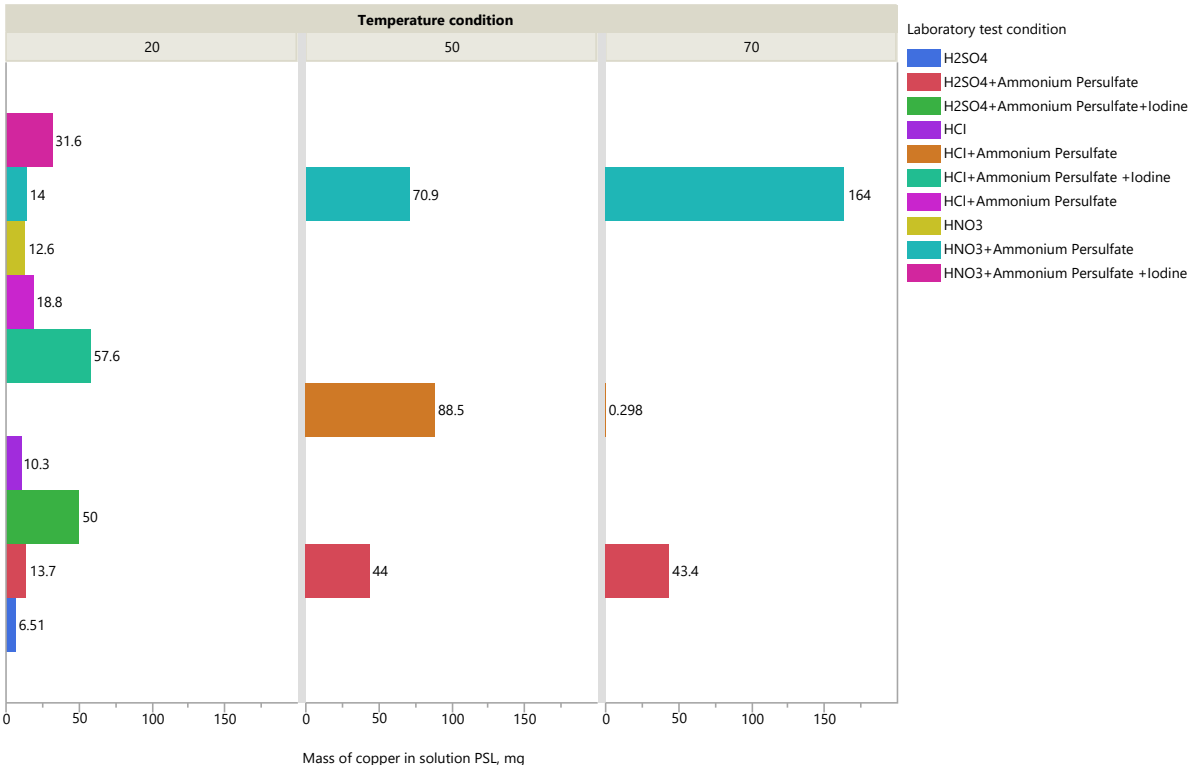


Figure 16. Mass of copper in PSL, mg

The mass of copper (mg) recovered in solution across different laboratory test conditions, categorized by three temperature levels: 20°C, 50°C, and 70°C. The study evaluates the efficacy of three primary acids—Sulfuric acid (H_2SO_4), Hydrochloric acid HCl), and Nitric acid (HNO_3)—both independently and in combination with additives such as Ammonium

There is a distinct positive correlation between temperature and copper dissolution. As the temperature increases from 20°C to 70°C, the leaching efficiency improves significantly for most chemical compositions.

The highest copper recovery was recorded at 70°C using the HCl **+** Ammonium Persulfate + Iodine system, yielding a peak mass of 164 mg. This indicates a strong synergistic effect between the chloride medium, the oxidizing agent (ammonium persulfate), and the catalyst (iodine) at elevated temperatures. In the 20°C range, the HNO_3 + Ammonium Persulfate + Iodine mixture showed the highest initial activity (57.6 mg). However, the HCl based systems demonstrated superior performance as the thermal energy increased, outperforming both H_2SO_4 and HNO_3 variants at 50°C and 70°C. Standard H2SO4 without

additives showed the lowest leaching capacity (6.51 mg at 20°C), highlighting the need for oxidizing agents to facilitate dissolution.

- **Copper Recovery Performance:**
    - A strong thermal dependency is observed, where the highest recovery rates are consistently achieved at 70°C.
    - The copper recovery peaks significantly at the 24-hour mark across all temperature gradients, with some data points at 70°C reaching nearly 90%.
    - At the lowest test temperature, recovery remains relatively stagnant, generally staying below 20% throughout the duration.
- **Iron (Fe) Dissolution Trends:**
    - The dissolution of iron follows a similar trend to copper, increasing proportionally with temperature.
    - At 70°C, the iron content in the solution stabilizes at a high range (50–65%), whereas at 20°C, it remains minimal (under 20%).
    - The sharp increase in iron content at the 24-hour sampling point suggests a period of intense chemical activity before potentially stabilizing or fluctuating in the subsequent hours.

The result shows that 70°C is the most effective temperature for maximizing copper recovery, although it also leads to higher iron dissolution. The 24-hour sampling interval appears to be a critical point for observing peak extraction efficiency in this specific experimental setup. The experimental data suggest that the kinetics of copper dissolution are highly dependent on the synergistic interaction between the chemical reagents and the thermal environment. The combination of Hydrochloric acid, Ammonium Persulfate, and Iodine at 70°C provides the most effective conditions for maximizing copper extraction.

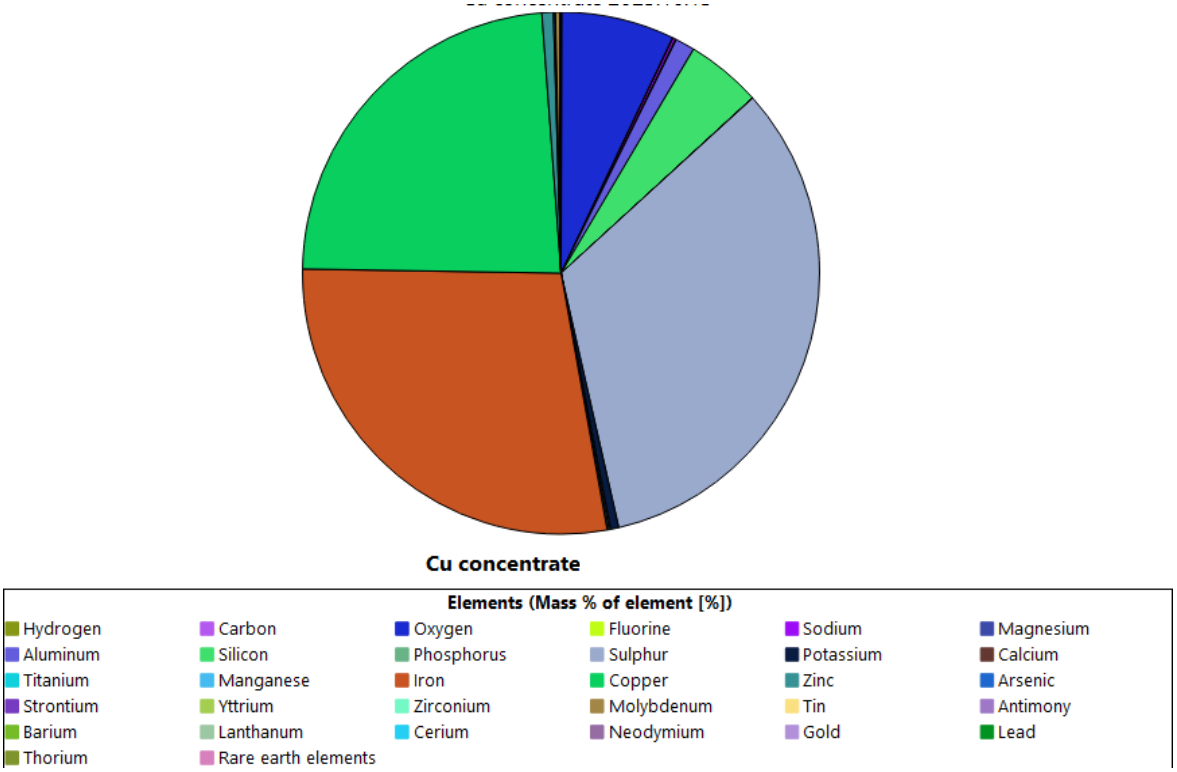


Table 11. Elemental mass of copper concentrate

The elemental composition of the copper concentrate confirms that the primary mineral matrix is chalcopyrite ($CuFeS_2$). The mass balance is dominated by Sulphur, Copper, and Iron, which collectively account for over 85% of the total mass. The presence of Silicon and Oxygen indicates silicate and oxide gangue minerals. This elemental profile justifies the use of a high-potential oxidant (Ammonium Persulfate) and Iodine catalysis to overcome the chemical stability of the iron-sulfur lattice during leaching.

Based on the mass analysis results, the primary constituents of the concentrate are Sulfur (S), Copper (Cu), and Iron (Fe), confirming that the sample is predominantly composed of the mineral chalcopyrite ($CuFeS_2$). The presence of Silicon (Si) and Oxygen (O) further indicates the inclusion of silicate-based gangue minerals.

- Dissolved Elements: Copper (Cu^{2+}) and iron (Fe^{2+}/Fe^{3+}) ions dissolve completely into the liquid phase under the influence of strong oxidants and the acidic medium.
- Solid Residue Constituents: Silicon (Si) and oxygen (O) remain in the solid tailings as inert silicates (e.g., SiO_2). Additionally, the elemental sulfur (S^0) generated during the leaching process forms a passivation layer on the mineral

surface; this layer persists until it is further oxidized to sulfate (SO_4^{2-}) by nitric acid (HNO_3).

1. The Role of Ammonium Persulfate ($(NH_4)_2S_2O_8$)

Ammonium Persulfate is a highly potent oxidant that accelerates the decomposition of chalcopyrite by releasing active oxygen into the solution. At 20°C, the oxidant lacks sufficient energy to penetrate the passivation layer of the chalcopyrite. However, as the temperature reaches 70°C, the reaction kinetics accelerate sharply, increasing copper recovery to 89.9%. The persulfate ion activates the mineral surface by accepting electrons and transforming into sulfate ions.

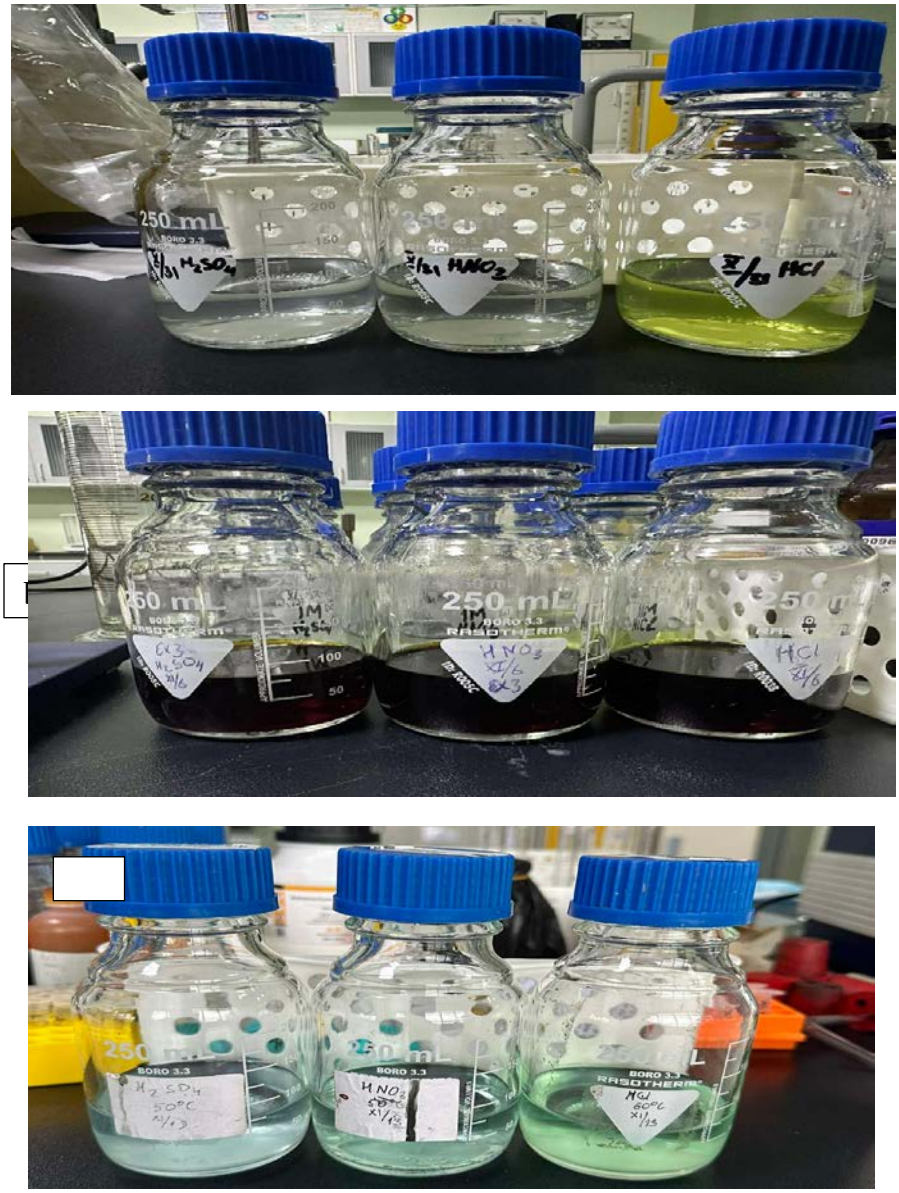


Figure 17. Experiment with ammonium persulfate

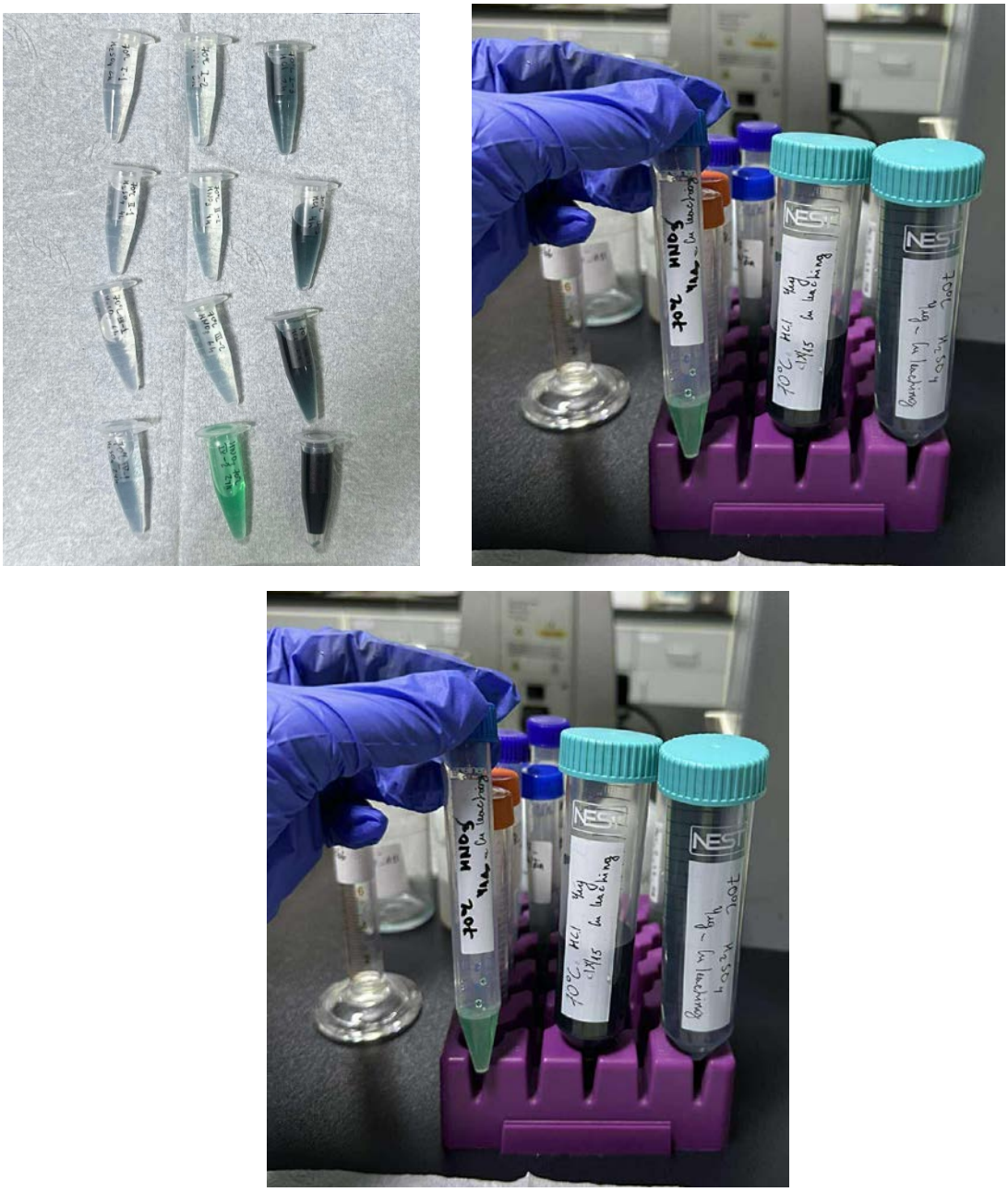


Figure 18. Sample of ammonium persulfate experiment

2. Comparison of Nitric Acid (HNO3) and Hydrochloric Acid (HCl)

Experimental results demonstrate that the type of acid used significantly influences the interaction with the oxidant. The HNO3 possesses inherent oxidizing properties, it works synergistically with Ammonium Persulfate to break down the sulfur-rich passivation layer most effectively.

Although HCl promotes ion transport by creating a chloride environment, copper recovery plateaued at approximately 74% at 50°C and did not reach the high efficiency observed with the nitric acid mixture.

Nitric acid possesses inherent oxidizing properties and works synergistically with Ammonium Persulfate to effectively break down the sulfur-rich passivation layer. In the presence of HNO_3, the elemental sulfur (S^0) that typically forms a resistive barrier on the mineral surface is further oxidized to sulfate (SO_4^{2-}), preventing passivation.

The oxidation of the sulfur layer by nitric acid:

$$S^0 + 6\mathrm{HN}O_3 \rightarrow H_2SO_4 + 6\mathrm{N}O_2 + 2H_2\mathrm{O} \quad (1)$$

Although HCl promotes ion transport by creating a chloride environment, copper recovery plateaued at approximately 74% at 50°C and did not reach the high efficiency observed with the nitric acid mixture. The chloride ions (Cl^-) facilitate the transport of metal ions by forming stable aqueous complexes, which stabilize copper in the solution:

Formation of copper-chloride complexes:

$$Cu^{2+} + 4\ Cl^- \rightarrow (CuCl_4)^{2-} \quad (2)$$

Overall leaching in chloride-persulfate media:

$$CuFeS_2 + 2\ S_2O_8^{2-} + n\ Cl^- \rightarrow [CuCl_n]^{2-n} + Fe^{2+} + 2\ S^0 + 4\ SO_4^{2-} \quad (3)$$

3. Effect of Iodine (I_2)

The addition of iodine was observed to improve copper recovery at low temperatures (20°C) to approximately 40%, which outperformed other reagent mixtures at the same temperature. Iodine acts as a catalyst by enhancing ion transport on the mineral surface. Thermal Limitation: As the temperature increases (50°C–70°C), the influence of the primary strong oxidants (persulfate and nitric acid) becomes dominant, and the relative catalytic benefit of iodine diminishes.

For the effective leaching of chalcopyrite, an acidic environment alone is insufficient. The synergistic combination of a high-potential oxidant (Ammonium Persulfate) and thermal energy (70°C) is the key to overcoming the mineral's natural resistance (passivation).

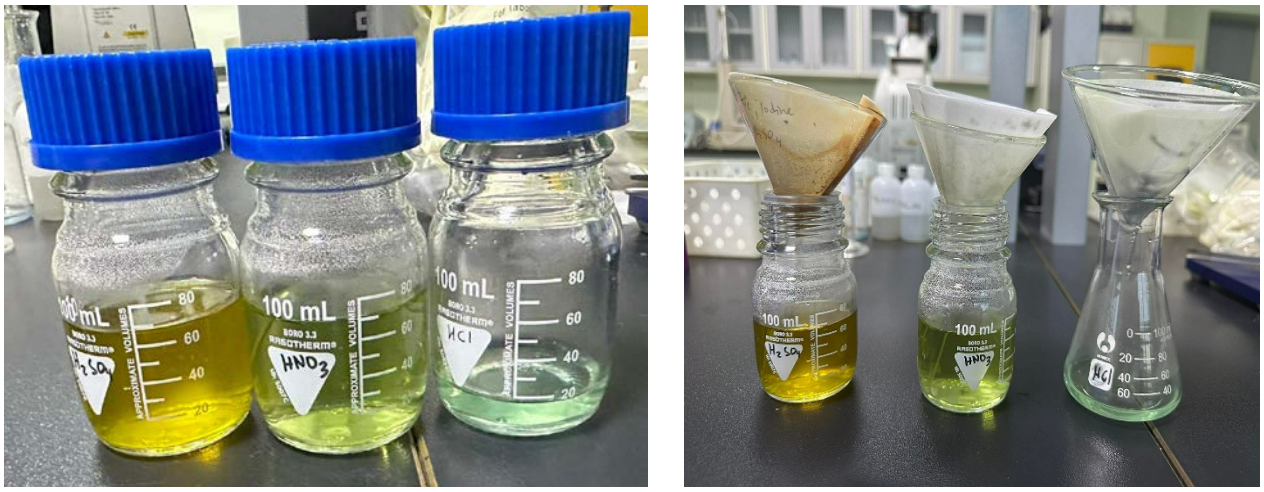


Figure 19.Experiment process of with iodine

The effective leaching of chalcopyrite requires more than just an acidic environment; it necessitates a synergistic combination of high-potential oxidants (Ammonium Persulfate) and thermal energy to overcome mineral passivation.

The oxidation of chalcopyrite by persulfate ions ($S_2O_8^{2-}$) is represented by the following equation:

$$CuFeS_2 + 2S_2O_8^{2-} \rightarrow Cu^{2+} + Fe^{2+} + 2S^0 + 4SO_4^{2-} \quad (4)$$

$$\mathrm{CuFe}S_2 + 2I_2 \rightarrow \mathrm{Cu}^{2+} + \mathrm{Fe}^{2+} + 2S^0 + 4I^- \quad (5)$$

$$2\,I^- + S_2O_8^{2-} \rightarrow I_2 + 2\,SO_4^{2-} \quad (6)$$

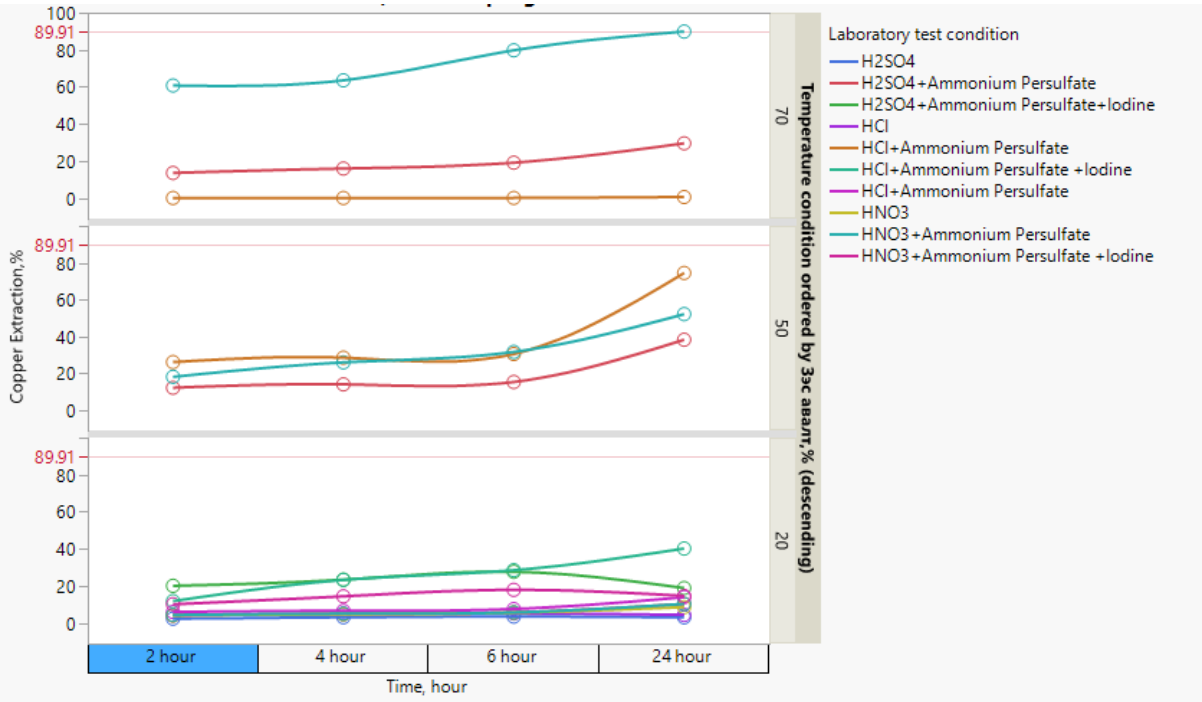


Figure 20. Effect of temperature and oxidizer on copper extraction leaching system

The kinetic analysis of chalcopyrite leaching reveals a pronounced synergistic effect between temperature and the oxidizing reagent system (HNO_3 + $(NH_4)_2S_2O_8$).

At 70 °C, the copper concentration in the pregnant leach solution (PLS) reached approximately 2001 mgL^{-1}, corresponding to an extraction efficiency of nearly 90%. The strong linearity of the Arrhenius plot ($R^2 \approx 1$) confirms the reliability of the calculated rate constants and demonstrates that the leaching kinetics follow Arrhenius behavior. The relatively high apparent activation energy derived from this relationship indicates that chalcopyrite dissolution under these conditions is governed primarily by surface chemical reaction steps rather than diffusion-controlled processes.

4.2 Effect of temperature

Experiments were conducted to determine the influence of different lixiviants on the leaching of copper concentrate while maintaining a constant temperature. In the second stage, oxidants that yielded positive results in the first stage were selected to evaluate the impact of increasing temperature. The results showed a significant effect; elevating the temperature rendered the solid surface more porous and made the surface sulfur layer thinner and more crystalline. The effect of temperature on chalcopyrite leaching was investigated at 20, 50 and 70 °C using ammonium persulfate–based oxidizing

systems. As shown in Figure 3.2, copper recovery increases markedly with increasing temperature for all investigated acid media.

This morphological change potentially enhances the reaction rate by improving the reduction of ferric ions (Fe3+) on the solid surface. Furthermore, it may facilitate the leaching reaction by promoting the decomposition of polysulfides, which are formed as intermediate products during the process.



Figure 21. The experiment temperature is getting up

In the third stage, the most favorable parameters from the second stage were selected. Upon further increasing the temperature, a sharp improvement in copper extraction was observed.

The leaching experiments were conducted at three distinct temperature levels: 20°C, 50°C, and 70°C. At 20°C, copper recovery remained relatively low, with the effect of the solvents insufficient (recovery rates below 20%).

In the HNO_3 + $(NH_4)_2S_2O_8$ system, copper recovery increased from approximately 10% at 20 °C to 52% at 50 °C, reaching nearly 90% at 70 °C after 24 h of leaching. This pronounced temperature dependence indicates that thermal energy plays a critical role in accelerating chalcopyrite dissolution by enhancing surface reaction rates and promoting the breakdown of passivation layers.

In contrast, the H_2SO_4 + $(NH_4)_2S_2O_8$ system exhibited a more moderate increase in recovery up to 50 °C, followed by a decrease at 70 °C. This behavior suggests that,

despite increased reaction kinetics at elevated temperatures, secondary phenomena such as elemental sulfur formation or iron-rich surface precipitates may partially inhibit further copper dissolution.

A comparison of copper recovery after 24 h at 50 °C for different acid media is presented in Figure 3.3. Among the investigated systems, the HCl + $(NH_4)_2S_2O_8$ leach achieved the highest copper recovery (~74%), followed by HNO_3 + $(NH_4)_2S_2O_8$ (~52%), while H_2SO_4 + $(NH_4)_2S_2O_8$ showed the lowest recovery (~38%).

The superior performance of the chloride-containing system can be attributed to the formation of soluble Cu–Cl complexes, which stabilize copper in solution and reduce surface passivation. In comparison, nitric acid provides a strongly oxidizing environment that enhances chalcopyrite oxidation, whereas sulfuric acid systems are more prone to surface passivation by sulfur and iron-bearing phases.

These results demonstrate that, in addition to temperature, the choice of acid medium significantly influences copper extraction efficiency, even under identical oxidant conditions.

The combined analysis of recovery–temperature relationships, acid medium comparisons, and Arrhenius kinetics suggests that chalcopyrite leaching in ammonium persulfate systems is controlled by chemically activated surface reactions. Elevated temperatures enhance oxidant effectiveness and facilitate the disruption of passivating surface layers, while the acid medium influences copper stabilization in solution and the extent of surface passivation. Overall, the HNO_3 + $(NH_4)_2S_2O_8$ system at elevated temperature (70°C) provides the most favorable conditions for chalcopyrite dissolution, achieving high copper recovery within practical leaching times.

CONCLUTIONS

This study evaluated the leaching efficiency of chalcopyrite-dominated copper concentrates using various oxidant-acid systems. Based on the experimental results, the following key conclusions were drawn.

The combination of nitric acid (HNO_3) and ammonium persulfate ($(NH_4)_2S_2O_8$) was identified as the most effective leaching system, achieving a copper recovery rate of

90% within 24 hours. This high efficiency is attributed to the synergistic effect between the two reagents:

- HNO3 facilitates the oxidation of Fe_2+ to Fe_3+.
- Ammonium persulfate generates sulfate radicals ($SO_4^{\cdot}$), which further intensify the decomposition of the mineral matrix.

Unlike traditional sulfuric acid systems, the HNO3-persulfate medium effectively prevented the formation of inhibitory passivation layers. This system offered the following advantages: increased solubility, resulting in more reaction products. It avoided precipitation issues and complex side reactions commonly encountered in chloride-based environments, thereby maintaining stable leaching kinetics.

Copper extraction was highly dependent on thermal and chemical parameters. Increasing the temperature to 70°C and optimizing the oxidant dosage significantly accelerated the reaction kinetics. In summary, this study demonstrates a highly effective and advantageous method for extracting copper from sulfide concentrates under laboratory conditions. This study demonstrates that chalcopyrite leaching in ammonium persulfate–based systems is strongly influenced by both temperature and acid medium. Copper recovery increased from approximately 10% at 20 °C to nearly 90% at 70 °C in the HNO_3 + $(NH_4)_2S_2O_8$ system after 24 h of leaching. Arrhenius analysis yielded a high apparent activation energy (≈84–85 kJ·mol^{-1}), indicating that the leaching process is governed predominantly by surface chemical reactions rather than diffusion control. Compared with conventional atmospheric leaching systems reported in the literature, the nitrate–persulfate system investigated in this work exhibits enhanced capability to overcome chalcopyrite passivation at moderate temperatures. These findings suggest that oxidant-assisted, low-pressure hydrometallurgical routes have significant potential for the efficient processing of chalcopyrite-rich copper concentrates.

CHAPTER 5: ECONOMIC EVALUATION

5.1 Scoping study for a copper hydrometallurgical plant

This chapter presents a preliminary economic assessment for an on-site hydrometallurgical facility using CESL technology (Concentrate Effluent Sulphide Leaching) combined with SX/EW (Solvent Extraction and Electrowinning). The facility

is designed to process 560,000 tpa (dry) of copper concentrate to produce 124 ktpa of Grade-A copper cathode. A preliminary net profit estimation for the further processing of copper concentrate via hydrometallurgical methods has been conducted.

- ✓ Copper price (LME cash): $13,060/t (Jan 2026 benchmark).
- ✓ Exchange rate: 3,558.57 mnt/usd.

At this unit cost, the facility would operate in the lower first quartile of the global copper cost curve, ensuring high profitability even during periods of price volatility.

5.1.1 Economies of Scale and Williams' Rule

The capital cost estimation utilizes the "Six-Tenths Rule" (Williams' Law), which posits that in chemical and metallurgical engineering, an increase in capacity does not lead to a linear increase in cost.

$$\text{CAPEXnew} = CAPEXref \times \left(\frac{Capacity_{new}}{Capacity_{ref}}\right)^{0.6}$$

Where:

- CAPEX_{new}: Estimated capital cost for the proposed plant capacity.
- CAPEX_{ref}:: Capital cost of the reference plant ($175 Million).
- Capacity_{new}:: Proposed production capacity (124 ktpa).
- Capacity_{ref}: Reference production capacity (100 ktpa).
- 0.6: The scaling exponent (Six-tenths rule), typical for metallurgical processing plants.

This allows the project to achieve a lower unit cost per ton by scaling production to 124.0 ktpa.

Cash Cost Analysis

The project's operational expenditure (OPEX) is analyzed using the Cash Cost metric. At $0.125/lb ($276/t), the facility is positioned in the first quartile of the global copper cost curve, ensuring high resilience against LME price fluctuations.

Capital and Operating Expenditure (CAPEX/OPEX)

Table 12. Total capital operating expenditure (CAPEX/OPEX)

Category	Allocation (%)	Value (USD Million)	Value (MNT Billion)
Primary Process Equipment	45%	89.6	319.0
Civil Works & Infrastructure	25%	49.8	177.2

Engineering & Management (EPCM)	15%	29.9	106.3
Contingency (15%)	15%	29.9	106.3
Total CAPEX	**100%**	**199.2**	**708.9**

The total capital expenditure (CAPEX) for the project is estimated at $199.2 million (708.9 billion MNT), based on 2026 international project appraisal benchmarks. The largest portion of the budget, 45% ($89.6 million), is allocated to primary process equipment, which represents the facility's high-value technological core. 25% ($49.8 million) of the total budget is dedicated to civil works and engineering infrastructure to ensure a robust foundation for plant operations. The remaining 30% is equally distributed between Engineering, Procurement, and Construction Management (EPCM) and Contingency, serving as a critical buffer against technical delays and market price volatility during the implementation phase.

5.1.2 Annual Operating Expenditure (OPEX) Breakdown

Based on a production of 273.59 million lbs/year (124 ktpa).

Cost Component	Unit Cost ($/lb)	Annual Total (USD M)	Share (%)
Electricity & Power	0.045	12.31	36%
Reagents & Consumables	0.035	9.58	28%
Labor & Salaries	0.015	4.10	12%
Maintenance & Spare Parts	0.020	5.47	16%
G&A (Admin & Other)	0.010	2.74	8%
Total OPEX	0.125	34.20	100%

With a total annual operating expenditure of $34.2 million and a unit cost of $0.125/lb, the project is positioned among the lowest-cost producers on the global copper cash cost curve. Labor and administrative costs combined account for only 20% of the total OPEX, indicating that the facility is highly automated, has low administrative overhead per unit, and achieves significant operational efficiency.

Civil Engineering and Infrastructure

The facility is designed as a modular industrial complex consisting of three primary structures:

Administrative & Staff Building: Housing the management offices, laboratory, control center, medical clinic, and canteen.

Cathode Production Workshop: A specialized sandwich-panel structure for the leaching and SX/EW circuits.

Copper Products Plant (Main Shop): A heavy industrial facility with a reinforced concrete foundation and a steel-framed sandwich-panel wall system. The lower 1.2m of the walls are reinforced with concrete blocks for mechanical protection. The roof truss height is set at 15.3m to accommodate overhead cranes.

Thermal Energy (Heat Supply)

To optimize operating costs, the facility will utilize waste heat (high-temperature steam) from the adjacent Sulfuric Acid Plant. Hot water requirements for staff facilities will be managed via electric boilers.

Table 13. Thermal energy demand

No	Building Name	Temp (°C)	Volume (m^3)	Total Load (Gcal/hr)
1	Copper Products Workshop	16	17,625.6	0.349
2	Cathode Production Plant	16	1,960.0	0.050
3	Administrative Building	18	2,812.0	0.057
Total				**0.455**

Electrical Power Supply

The total installed capacity is 924 kW. Power will be sourced from the 110/6 kV substation via a 6 kV overhead line. Two containerized substations (KTPN) with capacities of 630 kVA and located 4.5 km away and pumped to a 15 m^3 reservoir on the plant site.

Water Supply

Industrial and domestic water consumption is estimated at 40.8 m^3/hr. Water is sourced from a deep well located 4.5 km away and pumped to a 15 m^3 reservoir on the plant site

Human Resources and Organization

The plant will operate on a 3-shift, 8-hour continuous cycle for 330 days per year. The total workforce consists of 45 employees, with 80% dedicated to engineering and technical operations.

Table 14.Staffing structure

Unit	Position	Count	Total per Unit

Administration	Executive, Finance, HR, HSE	5	5
Cathode Plant	Technologists, Operators, Lab Techs	19	19
Copper Products	Engineers, Mechanics, Welders	15	15
Support Staff	General Maintenance, Helpers	6	6
GRAND TOTAL			**45**

located 4.5 km away and pumped to a 15 m³ reservoir on the plant site.

The facility is designed for continuous three-shift operations, with over 75% of the total 45 employees dedicated directly to the production and technological departments. Administrative and support staffing has been optimized to ensure that primary human resources are concentrated on highly skilled engineers, operators, and technical staff, thereby reducing overhead costs and maximizing operational efficiency.

5.2. Annual Net Profit Summary

Table 15. Consolidated Annual Net Profit Summary

Financial Metric	Value (USD)	Value (MNT)
Total Capital Expenditure (CAPEX)	$199.2 Million	708.9 Billion ₮
Annual Net Profit	$68.0 Million	241.9 Billion ₮
Annual Depreciation (15-year straight-line)	$13.28 Million	47.3 Billion ₮
Annual Cash Flow	$81.28 Million	289.2 Billion ₮

The project is estimated to generate a substantial annual cash flow of $81.28 million, which is the sum of the $68.0 million net profit and the $13.28 million non-cash depreciation expense. With a net profit margin of this magnitude, the project demonstrates an exceptional capacity to recover the initial investment, yielding a Simple Payback Period (SPP) of approximately 2.45 years when calculated against the annual cash flow.

$$SPP = \frac{Total\ CAPEX}{Annual\ Cash\ Flow} \approx 2.4\ years$$

The robust annual cash flow provides significant financial flexibility, allowing for rapid debt servicing if the project is leveraged, and ensuring high liquidity for future operational expansions or maintenance.

5.3 Environmental Significance (ESG)

Conventional H_2SO_4-based leaching systems are characterized by:

- High sulfuric acid consumption, leading to increased risk of acid handling, storage, and transportation incidents;
- The formation of large volumes of acidic effluents requiring extensive neutralization prior to discharge;
- Generation of iron-rich residues (e.g., jarosite, goethite), which often contain entrained sulfate and pose long-term stability concerns;
- Increased potential for acid mine drainage (AMD)–type reactions if residues are not properly managed.

Life-cycle assessment (LCA) studies have consistently shown that sulfuric acid production and neutralization contribute substantially to greenhouse gas emissions, water consumption, and chemical reagent intensity in copper hydrometallurgy. As a result, sulfuric acid–dominated flowsheets are increasingly scrutinized under modern environmental regulations and sustainability frameworks.

In contrast, ammonium persulfate–assisted leaching systems, particularly when combined with nitrate-based oxidants, offer several **environmental advantages** over conventional sulfuric acid routes.

Firstly, ammonium persulfate is a strong but transient oxidant that, upon reaction, decomposes primarily into sulfate ions. Unlike sulfuric acid–based systems, this process does not require continuous large-scale acid addition, thereby reducing total acid inventory and handling risks.

Secondly, international studies report that persulfate-assisted systems can achieve high copper extraction at **moderate temperatures and atmospheric pressure**, eliminating the need for autoclaves or oxygen injection. This results in:

- Lower energy demand,
- Reduced indirect CO_2 emissions,
- Improved operational safety.

Thirdly, the use of nitrate–persulfate systems has been shown to limit the formation of stable passivation layers, reducing the accumulation of problematic solid residues such as jarosite. Consequently, the solid waste generated tends to be more chemically stable and easier to neutralize, lowering long-term environmental liability.

Finally, ammonium-based reagents enable closed-loop nitrogen management strategies, in which ammonium ions can be recovered or biologically treated, further improving the process's overall environmental performance.

Comparative environmental assessment

When compared on a functional basis (kg Cu produced), ammonium persulfate–based leaching systems demonstrate:

- Lower net acid consumption,
- Reduced effluent neutralization demand,
- Lower solid waste hazard potential, and
- Improved alignment with green hydrometallurgy principles emphasized in recent international literature.

These findings are consistent with global trends toward minimizing aggressive mineral acids and adopting **selective, high-efficiency oxidant systems** that achieve metallurgical objectives while reducing environmental burden.

The results of this study, in combination with international environmental assessments, indicate that ammonium persulfate–assisted chalcopyrite leaching represents a more environmentally benign alternative to traditional sulfuric acid–based technologies. By reducing acid intensity, secondary waste generation, and energy requirements, such systems support the transition toward sustainable and responsible copper production, particularly in regions where water management and long-term residue stability are critical concerns.

Compared with conventional sulfuric acid–based hydrometallurgical technologies, the ammonium persulfate–assisted leaching system investigated in this study demonstrates a substantially lower potential environmental impact, primarily due to reduced acid consumption, lower secondary waste generation, and improved compatibility with sustainable hydrometallurgical practices reported in international literature.

SUMMARY

This research focuses on identifying innovative methods to enhance the leaching kinetics of chalcopyrite ($CuFeS_2$), the primary mineral component of copper concentrates. A central objective of the study is to develop environmentally sustainable

methodologies that minimize ecological impact while maximizing metal extraction. Chalcopyrite is notoriously refractory due to its high chemical stability under ambient conditions; a significant bottleneck in its processing is the formation of a "passivation layer" during leaching, which acts as a diffusional barrier and severely restricts copper recovery.

The study was executed across three thermal gradients (20°C, 50°C, and 70°C) to evaluate the performance of different acidic media (H_2SO_4, HCl, and HNO3). These lixiviant systems were tested in conjunction with ammonium persulfate $(NH_4)_2 S_2O_8$) as a high-potential oxidant and molecular iodine (I2) as a catalytic mediator. The kinetic behavior of copper and iron dissolution was monitored over a 24-hour sampling period to determine the optimal leaching configuration.

Optimal Leaching System: Experimental results demonstrate that the HCl + Ammonium Persulfate + Iodine system achieved peak efficiency at 70°C, yielding 164 mg of dissolved copper and reaching a metal recovery rate of 90%. This superior performance is attributed to the synergistic interaction between chloride-mediated complexation and the iodine catalytic cycle.

Thermal Influence: It was confirmed that increasing the temperature effectively lowers the activation energy barrier for mineral decomposition, leading to a sharp acceleration in dissolution rates. While recovery remained marginal (below 20%) at 20°C, the system reached its maximum efficacy at 70°C.

Role of Iodine Catalysis: Iodine acts as a surface-active agent that facilitates electron transfer. It mitigates the effects of passivation by either increasing the porosity of the elemental sulfur layer or promoting its total degradation, thereby maintaining reagent access to the mineral interface.

The research data support the electronic model of chalcopyrite consisting of monovalent copper (Cu+) and trivalent iron (Fe3+). Defining these formal valence states in covalent sulfide matrices is essential for interpreting the fundamental kinetics of the mineral's breakdown.

For the hydrometallurgical extraction of copper from chalcopyrite concentrates, the combination of hydrochloric acid, persulfate, and iodine at elevated temperatures offers the most robust technological pathway. This innovative approach provides a sustainable alternative for the industry by reducing overall energy consumption and

significantly increasing copper output, marking a new advancement in green extractive metallurgy.

The most significant result of the study was the combination of Nitric acid (HNO_3) and ammonium persulfate ($(NH_4)_2S_2O_8$). This system achieved 90% copper recovery within 24 hours at 70°C, significantly outperforming all other tested mixtures.

The reason for the high efficiency lies in the interaction between the two reagents:

Nitric acid: Oxidizes iron ions ($Fe^{2+} \rightarrow Fe^{3+}$) and promotes mineral decomposition.

Ammonium persulfate: Generates strong oxidizing radicals and directly breaks down the passivation layer on the surface of chalcopyrite.

Iodine (I_2): Iodine acts as a "bridge" for electron transfer between the mineral surface and the bulk oxidant (ammonium persulfate). Unlike bulk oxidants that may struggle to penetrate the mineral interface, iodine reacts directly with the chalcopyrite lattice to release metal ions while being reduced to iodide (I-).

Experiments confirmed that temperature has a direct impact on the leaching rate :

- ✓ 20°C: Copper recovery below 20% (chalcopyrite is highly resistant at room temperature).
- ✓ 50°C: The process intensified, reaching 74% in the HCl mixture.
- ✓ 70°C: The optimal temperature, providing sufficient energy to the system to decompose the passivation layer.

Compared to traditional sulfuric acid methods, this system:

- Does not inhibit leaching by forming elemental sulfur precipitates.
- Maintains a stable copper recovery rate due to the high solubility of reaction products.

This research work has identified and confirmed an efficient method for processing refractory ores and concentrates in a short period.

In terms of economic feasibility, Traditional sulfuric acid leaching often fails to achieve viable recovery rates due to the rapid formation of a passivation layer on the chalcopyrite ($CuFeS_2$) surface. In contrast, this study's optimized method achieves a 90% copper recovery rate. By increasing the final product output by approximately 2-2.2-2.5 times from the same volume of raw material, the project secures a robust financial foundation, justifying the projected annual net profit of 68$ million. This high

recovery rate directly enhances the marginal profit by keeping raw material costs constant while maximizing top-line revenue.

Compared to traditional smelting (pyrometallurgy) or high-acid pressure leaching, this "Green Metallurgy" approach minimizes toxic gas emissions and reduces the ecological footprint. By aligning with global Environmental, Social, and Governance (ESG) standards, the project:

- Mitigates future financial liabilities related to environmental remediation and carbon taxes.
- Positions the final product as "Green Copper" which may command a premium price in international markets increasingly focused on sustainable supply chains.

The technological solution validated by this research is not only technically superior but also financially compelling. With a high Return on Investment (ROI) and low operational risk, it provides a stable and profitable pathway for the industrial-scale processing of refractory copper concentrates.

REFERENCES

1. Cerda, C., Taboada, M., Jamett, N., Ghorbani, Y., & Hernández, P. (2017). Effect of Pretreatment on Leaching Primary Copper Sulfide in Acid-Chloride Media. *Minerals*, *8*(1), 1. Https://doi.org/10.3390/min8010001
2. Chmielewski, T., & Kaleta, R. (n.d.). *Galvanic interactions of sulfide minerals in leaching of flotation concentrate from lubin concentrator*.
3. Clark, M. E., Batty, J. D., Van Buuren, C. B., Dew, D. W., & Eamon, M. A. (2006). Biotechnology in minerals processing: Technological breakthroughs creating value. *Hydrometallurgy*, *83*(1–4), 3–9. Https://doi.org/10.1016/j.hydromet.2006.03.046
4. Crowson, P. (2012). The copper industry: Challenges of the last 40 years. *Resources Policy*, *37*, 59–72.
5. *EMC, Technological instruction*. (2024).
6. Franklin, J. M., Gibson, H. L., & Jonasson, I. R. (n.d.). *Volcanogenic Massive Sulfide Deposits*.
7. Fuerstenau, M. C., & Han, K. N. (Eds.). (2009). *Principles of mineral processing*. Society for Mining, Metallurgy, and Exploration.
8. Koleini, S. M. J., Aghazadeh, V., & Sandström, Å. (2011). Acidic sulphate leaching of chalcopyrite concentrates in presence of pyrite. *Minerals Engineering*, *24*(5), 381–386. Https://doi.org/10.1016/j.mineng.2010.11.008
9. Lundström, M. (n.d.). *Chalcopyrite dissolution in cupric chloride solutions*.
10. Nakajima, K., Daigo, I., Nansai, K., Matsubae, K., Takayanagi, W., Tomita, M., & Matsuno, Y. (2018). Global distribution of material consumption: Nickel, copper, and iron. *Resources, Conservation and Recycling*, *133*, 369–374. Https://doi.org/10.1016/j.resconrec.2017.08.029
11. Oxdizationstep, R. (n.d.). *Iron (ii) ion solution replacement*.
12. Patnaik, P. (2003). *Handbook of inorganic chemicals*. Mcgraw-Hill.
13. Qicheng Feng and Guang Han. (n.d.). *Advances in Flotation of Copper, Lead and zinc Minerals*. Mdpi.com/journal/minerals
14. Ruiz, M. C., Montes, K. S., & Padilla, R. (2015). Galvanic Effect of Pyrite on Chalcopyrite Leaching in Sulfate-Chloride Media. Mineral Processing and

Extractive Metallurgy Review, 36(1), 65–70. Https://doi.org/10.1080/08827508.2013.868349

15. Schipper, B. W., Lin, H. C., Meloni, M. A., Wansleeben, K., Heijungs, R., & van der Voet, E. (2018). Global material flows of copper and its environmental impacts. *Resources, Conservation and Recycling*, 28–36.
16. Schlesinger, M. E. (Ed.). (2011). *Extractive metallurgy of copper*. Elsevier.
17. Sillitoe, R. H. (2010). Porphyry Copper Systems*. *Economic Geology*, *105* (1), 3–41. Https://doi.org/10.2113/gsecongeo.105.1.3
18. Singer, D. A. (2017). Future copper resources based on geological models. *Ore Geology Reviews*, *86*, 271–279.
19. Srdjan M. Bulatovic. (n.d.). *Flotation of copper sulfide ores*.
20. *The kinetics of the dissolution of chalcophyrite (2)*. (n.d.).
21. Yang, Y., Yang, G., Xu, W., Wang, X., Song, J., & Zhu, T. (2025). Study on oxidative leaching of multi-component in copper anode slime enhanced by hydrogen peroxide. *Separation and Purification Technology*, *361*, 131635. Https://doi.org/10.1016/j.seppur.2025.131635
22. Chmielewski, T., & Kaleta, R. (n.d.). *Oxidation of sulfide minerals in hydrometallurgy.*
23. Dutrizac, J. E. (1990). The dissolution of chalcopyrite in ferric sulfate and ferric chloride media. *Metallurgical Transactions B, 21*(2), 301–317.
24. Gericke, M., Pinches, A., & van Rooyen, J. V. (2001). Bioleaching of a chalcopyrite concentrate using an extremely thermophilic culture. *International Journal of Mineral Processing, 62*(1-4), 243–255.
25. Klauber, C., et al. (2001). Sulphur and iron oxidation states during the surface oxidation of chalcopyrite. *International Journal of Mineral Processing, 62*(1-4), 171–194.
26. Cordoba, E. M., Muñoz, J. A., Blázquez, M. L., González, F., & Ballester, A. (2008). Leaching of chalcopyrite with ferric ion. Part I: General aspects. *Hydrometallurgy, 93*(3-4), 81–87.
27. Chmielewski, T., & Kaleta, R. (n.d.). *Oxidation of sulfide minerals in hydrometallurgy.*

28. Rao, et al. (2024). Surface chemistry and flotation behavior of complex sulfide minerals. *International Journal of Mineral Processing.*
29. Zhang, & Honaker. (2023). Evaluation of galvanic interaction on the flotation of sulfide minerals. *Powder Technology.*
30. Jiang, L., Leng, H., & Han, B. (2023). Dissolution and Passivation Mechanism of Chalcopyrite during Pressurized Water Leaching. *Minerals*, *13*(8), 996. https://doi.org/10.3390/min13080996
31. Blank, L. T., & Tarquin, A. J. (2021). *Engineering economy* (9th ed.). McGraw-Hill Education.
32. Dreisinger, D. (2006). Copper leaching from chalcopyrite: A review. *Hydrometallurgy, 83*(1-4), 10–20. https://doi.org/10.1016/j.hydromet.2006.03.017
33. International Copper Study Group (ICSG). (2025). *World Copper Factbook 2025*. https://www.icsg.org
34. Marsden, J. O. (2006). *Hydrometallurgy of copper*. Society for Mining, Metallurgy, and Exploration (SME).
35. Williams, R. (1947). "Six-tenths factor" aids in approximating costs. *Chemical Engineering, 54*(12), 124–125.